

Gravitational waves from inspiraling black holes in quadratic gravity

Matheus F. S. Alves,^{1,2,*} Luís F. M. A. M. Reis,^{1,†} and L. G. Medeiros^{3,‡}

¹*Departamento de Física Teórica e Experimental,*

Universidade Federal do Rio Grande do Norte, Natal, RN, 59078-970, Brazil.

²*Departamento de Física, Universidade Federal do Espírito Santo, Vitória, ES, 29075-910, Brazil.*

³*Escola de Ciência e Tecnologia, Universidade Federal do Rio Grande do Norte, Campus Universitário, s/n-Lagoa Nova, CEP 59078-970, Natal, Rio Grande do Norte, Brazil.*

We perform a study of gravitational waves emitted by inspiraling black holes in the context of quadratic gravity. By linearizing the field equations around a flat background, we demonstrate that all degrees of freedom satisfy wavelike equations. These degrees of freedom split into three modes: a massive spin-2 mode, a massive spin-0 mode, and the expected massless spin-2 mode. We construct the energy-momentum tensor of gravitational waves and show that, due to the massive spin-2 mode, it presents the Ostrogradsky instability. We also show how to deal with this possible pathology and obtain consistent physical interpretations for the system. Using the energy-momentum tensor, we study the influence of each massive mode in the orbital dynamics and compare it with the standard result of general relativity. Moreover, we present two methods to constrain the parameter α associated with the massive spin-2 contribution. From the first method, using the combined waveform for the spin-2 modes, we obtain the constraint $\alpha \lesssim 1.1 \times 10^{21} m^2$. In the second method, using the coalescence time, we get the constraint $\alpha \lesssim 1.1 \times 10^{13} m^2$.

I. INTRODUCTION

The direct detections of gravitational waves (GWs) by the LIGO-VIRGO collaboration, first in 2015 due to the collision of two black holes and then in 2017 due to the collision of two neutron stars, is one of the main results in the history of general relativity (GR) [1–3]. These detections not only observationally confirm one of the fascinating results of GR but also make it possible to obtain a deeper understanding of the gravitational interaction. In addition to the direct detections, GWs had already been indirectly observed through neutron star binary systems. In the 1970s, Hulse and Taylor observed a decrease in the orbital period of the PSR 1913+16 system [4], entirely consistent with the energy and momentum losses predicted by GR theory due to GWs emission [5, 6].

Despite these and several other experimental results supporting the GR, there is a consensus in the scientific community that it is an incomplete theory. In addition to some structural problems within the theory, such as the presence of singularities, the GR also presents problems when analyzed in the context of high-energy physics. general relativity cannot be quantized through the conventional methods of particle physics [7, 8], and it struggles to describe the early (inflationary) universe consistently [9, 10].

One of the main approaches to solving these problems is modifying the GR, especially the Einstein-Hilbert action. The first proposal to modify GR, and in turn the simplest, came from Einstein himself, who introduced the cosmological constant Λ in theory as a way of solving the cosmological view of his time [11]. Despite being one of

the main candidates for dark energy, this modification still faces some observational problems that may even be associated with the current "cosmological crisis" [12–19].

There are, however, more sophisticated modification proposals which involve the addition of the curvature scalar terms, such as the $f(R)$ theories [20–23]. In this scenario, the theory $f(R) = R + \alpha R$, for example, constitutes the so-called Starobinsky inflationary model [9, 24], which proves to be a consistent approach to inflation [25]. Besides $f(R)$ theories, there are proposals for several other modifications to the Einstein-Hilbert action, e.g. theories that include a vector field [26–28] and theories involving the addition of higher-order terms like ∇R , $\nabla^n R$ and $R \square R$ [29–31]. Therefore, the search for observational constraints in modified theories of gravity proves to be fundamental in attempting to narrow down the parameters of these theories.

One of the main ways of establishing observational constraints in theories of modified gravity is in the cosmological context [32–35]. However, with the new era of GWs detection, the analysis of modified theories in contexts of gravitational waves [36–41] is also of great interest, even allowing the determination of parameters in new scales different from those probed in cosmology [42–46].

In this spirit, we analyze the quadratic gravity model given by the action (1) in the context of the emission of gravitational waves:¹

$$S = \int d^4x \sqrt{-g} \left[R + \frac{1}{2} \gamma R^2 - \frac{1}{2} \alpha C_{\mu\nu\alpha\beta} C^{\mu\nu\alpha\beta} \right] \quad (1)$$

$$- 2\kappa \int d^4x \sqrt{-g} \mathcal{L}_m,$$

* matheus.s.alves@edu.ufes.br

† luisfmmreis@gmail.com

‡ leo.medeiros@ufrn.br

¹ These action was proposed by Stelle [47, 48] to deal with the renormalizability problem of the gravitational field.

where $\kappa = \frac{8\pi G}{c^4}$, α , γ are coupling constants with the dimension of (length)² and $C_{\mu\nu\alpha\beta}$ is the Weyl tensor.

Quadratic gravity is embedded in a context of higher-order gravity theories where higher energy corrections are inserted in the action. In this context, the Einstein-Hilbert term and the cosmological constant are zero-order terms (squared mass terms), the invariants R^2 and $C_{\mu\nu\alpha\beta}C^{\mu\nu\alpha\beta}$ are first-order corrections² (fourth mass terms), quantities of the type $R\Box R$, $C_{\mu\nu\alpha\beta}\Box C^{\mu\nu\alpha\beta}$ plus cubic terms in the Riemann tensor are second-order corrections (sixth mass terms), etc.³ Thus, this work aims to study how first-order corrections to general relativity influence the emission of GWs emitted by binary systems. More specifically, we study the emission of GWs produced by the inspiral phase of a binary black hole system in the approximations of point masses, circular orbit, and nonrelativistic dynamics.

The paper has the following structure: in Sec. II, we carry out the linearization of the field equation decomposing the metric into three new fields: a massless spin-2

field, as in GR; a massive spin-2 field, and a massive spin-0 field. Next, we analyze the gauge conditions that allow us to reduce the degrees of freedom of these new fields significantly. In the Sec. III, we obtain the Green's functions for the massive fields and carefully analyze the multipolar expansion for each field. In Sec. IV, the solutions of the fields in terms of the multipolar expansions are applied to a binary system of point masses in circular orbits and the power radiated by the GWs is obtained. With that, in Sec. V, the effect of the emission of GWs is analyzed using the energy balance equation, so that the inspiral phase is studied in terms of the orbital frequency of the system. In addition, Ostrogradsky's instability, generated by the Weyl-Weyl term, is carefully analyzed in this section, and then it is shown how this apparent pathology can be suppressed and corrected. In light of this apparent pathology, we discuss in Sec. VI the role that spin-2 fields play in the emission of GWs, mainly explaining the differences and similarities between these fields, such as their propagation velocities and waveforms. With this, we establish some observational constraints. Finally, we end with the final comments in the Sec. VII.

II. QUADRATIC GRAVITY IN THE WEAK-FIELD REGIME

The field equation is obtained from (1) by varying it with respect to $g^{\mu\nu}$:

$$R_{\mu\nu} - \frac{1}{2}g_{\mu\nu}R + \gamma \left[R \left(R_{\mu\nu} - \frac{1}{4}Rg_{\mu\nu} \right) + g_{\mu\nu}\nabla_\rho\nabla^\rho R - \nabla_\mu\nabla_\nu R \right] - \alpha \left[\nabla^\rho\nabla^\beta C_{\mu\rho\nu\beta} + \frac{1}{2}R^{\rho\beta}C_{\mu\rho\nu\beta} \right] = \kappa T_{\mu\nu} \quad (2)$$

with the Riemann and Weyl tensors defined as

$$R^\kappa{}_{\nu\alpha\beta} \equiv \partial_\alpha\Gamma^\kappa{}_{\nu\beta} - \partial_\beta\Gamma^\kappa{}_{\nu\alpha} + \Gamma^\kappa{}_{\rho\alpha}\Gamma^\rho{}_{\nu\beta} - \Gamma^\kappa{}_{\rho\beta}\Gamma^\rho{}_{\nu\alpha}, \quad (3)$$

$$C_{\mu\nu\alpha\beta} \equiv R_{\mu\nu\alpha\beta} - \frac{1}{2}(g_{\mu\alpha}R_{\beta\nu} - g_{\mu\beta}R_{\alpha\nu} + g_{\nu\beta}R_{\alpha\mu} - g_{\nu\alpha}R_{\beta\mu}) + \frac{1}{6}R(g_{\mu\alpha}g_{\beta\nu} - g_{\mu\beta}g_{\alpha\nu}). \quad (4)$$

In addition, the trace of the field equation (2) is

$$3\gamma\nabla_\rho\nabla^\rho R - R = \kappa T. \quad (5)$$

The linearized equations on a flat background for quadratic gravity were obtained in Ref. [50]. However, we will retrieve these equations using a clearer and more simplified approach. We start by decomposing the metric as⁴

$$g_{\mu\nu} = \eta_{\mu\nu} + h_{\mu\nu},$$

where $|h_{\mu\nu}| \ll 1$. From the definition of the trace-reverse tensor $h_{\nu\beta} = \bar{h}_{\nu\beta} - \frac{1}{2}\eta_{\nu\beta}\bar{h}$, we obtain in linear order

$$\begin{aligned} C_{\mu\nu\alpha\beta}^{(1)} = & \frac{1}{2} [\partial_\alpha\partial_\nu\bar{h}_{\mu\beta} - \partial_\beta\partial_\nu\bar{h}_{\mu\alpha} + \partial_\beta\partial_\mu\bar{h}_{\nu\alpha} - \partial_\alpha\partial_\mu\bar{h}_{\nu\beta}] \\ & - \frac{1}{4}\eta_{\mu\alpha} (\partial_\rho\partial_\nu\bar{h}^\rho{}_\beta - \partial_\beta\partial_\nu\bar{h} + \partial_\beta\partial_\rho\bar{h}_\nu{}^\rho - \Box\bar{h}_{\nu\beta}) \\ & + \frac{1}{4}\eta_{\mu\beta} (\partial_\rho\partial_\nu\bar{h}^\rho{}_\alpha - \partial_\alpha\partial_\nu\bar{h} + \partial_\alpha\partial_\rho\bar{h}_\nu{}^\rho - \Box\bar{h}_{\nu\alpha}) \\ & - \frac{1}{4}\eta_{\nu\beta} (\partial_\rho\partial_\mu\bar{h}^\rho{}_\alpha - \partial_\alpha\partial_\mu\bar{h} + \partial_\alpha\partial_\rho\bar{h}_\mu{}^\rho - \Box\bar{h}_{\mu\alpha}) \\ & + \frac{1}{4}\eta_{\nu\alpha} (\partial_\rho\partial_\mu\bar{h}^\rho{}_\beta - \partial_\beta\partial_\mu\bar{h} + \partial_\beta\partial_\rho\bar{h}_\mu{}^\rho - \Box\bar{h}_{\mu\beta}) \\ & + \frac{1}{6} [\partial_\sigma\partial_\rho\bar{h}^{\sigma\rho} - \Box\bar{h}] (\eta_{\mu\alpha}\eta_{\beta\nu} - \eta_{\mu\beta}\eta_{\alpha\nu}), \end{aligned} \quad (6)$$

² The other two first-order terms, namely $\Box R$ and $G = R^2 - 4R_{\mu\nu}R^{\mu\nu} + R_{\mu\nu\alpha\beta}R^{\mu\nu\alpha\beta}$, do not contribute to the field equations.

³ More details about this construction can be found in the introduction of [49].

⁴ We adopted the $(-1, 1, 1, 1)$ signature for the metric.

and

$$R_{\mu\nu}^{(1)} \approx \frac{1}{2} \left[\partial_\rho \partial_\nu \bar{h}_\mu{}^\rho + \partial_\rho \partial_\mu \bar{h}_\nu{}^\rho - \square \bar{h}_{\mu\nu} + \frac{1}{2} \eta_{\mu\nu} \square \bar{h} \right], \quad (7)$$

$$R^{(1)} \approx \partial_\sigma \partial_\rho \bar{h}^{\sigma\rho} + \frac{1}{2} \square \bar{h} \quad (8)$$

where $\square \equiv \partial_\alpha \partial^\alpha$ and $\bar{h} \equiv \bar{h}^\alpha{}_\alpha$.

The objective is to obtain wave equations for the various degrees of freedom of the metric in quadratic gravity. We start by defining the dimensionless scalar quantity $\Phi \equiv -\gamma R^{(1)}$. In this case, the linearized equation (5) can be written as

$$(\square - m_\Phi^2) \Phi = -\frac{\kappa T}{3}, \quad (9)$$

where $m_\Phi^2 = 1/(3\gamma)$ and T is the trace of $T_{\mu\nu}$ in its linearized form. Then we decompose the metric into a scalar part and a tensorial part [51, 52]

$$\bar{h}_{\mu\nu} = \Theta_{\mu\nu} - \eta_{\mu\nu} (\Phi + \phi) \quad (10)$$

with ϕ representing an auxiliary gauge field⁵. Further-

more, for the spin-2 part, we adopt the gauge

$$\partial^\nu \Theta_{\mu\nu} = 0 \Rightarrow \partial^\nu \bar{h}_{\mu\nu} = -\partial_\mu (\Phi + \phi). \quad (11)$$

Substituting the decomposition (10) in the linearized equation (2) we get

$$\square \Theta_{\mu\alpha} + 2\partial_\mu \partial_\alpha \phi - 2\eta_{\mu\alpha} \square \phi + 2\alpha \partial^\nu \partial^\beta C_{\mu\nu\alpha\beta}^{(1)} = -2\kappa T_{\mu\alpha}. \quad (12)$$

The next step is to separate the tensorial component into a massive and a nonmassive mode:

$$\Theta_{\mu\alpha} = \tilde{h}_{\mu\alpha} + \Psi_{\mu\alpha}, \quad (13)$$

where we impose that the nonmassive mode $\tilde{h}_{\mu\alpha}$ satisfies the equation

$$\square \tilde{h}_{\mu\alpha} = -2\kappa T_{\mu\alpha}. \quad (14)$$

Thus, Eq. (12) can be rewritten as

$$\square \Psi_{\mu\alpha} + 2\partial_\mu \partial_\alpha \phi - 2\eta_{\mu\alpha} \square \phi + 2\alpha \partial^\nu \partial^\beta C_{\mu\nu\alpha\beta}^{(1)} = 0. \quad (15)$$

Then, we use the decomposition of the metric in the Weyl tensor and calculate $\partial^\nu \partial^\beta C_{\mu\nu\alpha\beta}^{(1)}$ obtaining

$$\partial^\nu \partial^\beta C_{\mu\nu\alpha\beta}^{(1)} = -\frac{1}{4} \square^2 (\tilde{h}_{\mu\alpha} + \Psi_{\mu\alpha}) + \frac{1}{12} \eta_{\mu\alpha} \square^2 (\tilde{h} + \Psi) - \frac{1}{12} \partial_\alpha \partial_\mu \square (\tilde{h} + \Psi),$$

where $\tilde{h} \equiv \tilde{h}^\alpha{}_\alpha$ and $\Psi \equiv \Psi^\alpha{}_\alpha$.

Once $\partial^\nu \partial^\beta C_{\mu\nu\alpha\beta}^{(1)}$ has been calculated, we substitute this result in (15) and choose the gauge field ϕ as⁶

$$\phi = \frac{\alpha}{3} \square (\tilde{h} + \Psi). \quad (16)$$

So, Eq. (15) is rewritten as

$$\square \left[\Psi_{\mu\alpha} - \frac{\alpha}{2} \square (\tilde{h}_{\mu\alpha} + \Psi_{\mu\alpha}) \right] = 0. \quad (17)$$

For trivial boundary conditions (e.g. fields vanishing at infinity), the above equation is satisfied only if the term in square brackets is null. In this case, using Eq. (14) we get

$$(\square - m_\Psi^2) \Psi_{\mu\alpha} = 2\kappa T_{\mu\alpha}, \quad (18)$$

where $m_\Psi^2 = 2/\alpha$. From the field equations (14) and (18) we can show that the gauge conditions (11) and (16) result in

$$\partial^\mu \Psi_{\mu\nu} = 0, \quad \partial^\mu \tilde{h}_{\mu\nu} = 0 \quad \text{and} \quad \phi = \frac{1}{3} \Psi. \quad (19)$$

Therefore, the decomposition of the metric in the form

$$\bar{h}_{\mu\nu} = \tilde{h}_{\mu\nu} + \Psi_{\mu\nu} - \eta_{\mu\nu} \left(\Phi + \frac{1}{3} \Psi \right), \quad (20)$$

and the choice of gauge (19) result in the Eqs. (9), (14) and (18) associated with massive spin-0, massless spin-2 and massive spin-2 degrees of freedom, respectively.

A. Degrees of freedom

As in general relativity, the conditions given in (19) do not completely fix the gauge. Performing an infinitesimal coordinate transformation

$$x'^\mu = x^\mu + \xi^\mu(x),$$

it is possible to show that the full spin-2 mode transforms as

$$\Theta'_{\mu\nu} = \Theta_{\mu\nu} - \partial_\mu \xi_\nu - \partial_\nu \xi_\mu + \eta_{\mu\nu} \partial^\beta \xi_\beta. \quad (21)$$

Taking the divergence of the expression above, we notice that any transformation ξ_ν that respects $\square \xi_\nu = 0$ maintains the harmonic gauge $\partial^\mu \Theta_{\mu\nu} = 0$. This residual

⁵ The Φ field contains the entire scalar degree of freedom of the metric.

⁶ This choice is necessary to obtain a wave equation for $\Psi_{\mu\alpha}$.

gauge freedom allows us to choose a transformation in the form

$$\xi_\nu = b_\nu e^{i\bar{k}_\alpha x^\alpha} + b_\nu^* e^{-i\bar{k}_\alpha x^\alpha}, \quad (22)$$

where $\bar{k}_\alpha \bar{k}^\alpha = 0$ and b_ν is an arbitrary constant vector.

The next step is to show that this extra degree of freedom, incorporated in the b_ν vector, acts only in massless spin-2 modes. This can be verified from the vacuum solutions of Eqs. (14) and (18)

$$\tilde{h}_{\mu\nu} = \tilde{\varepsilon}_{\mu\nu} e^{ik_\alpha x^\alpha} + \tilde{\varepsilon}_{\mu\nu}^* e^{-ik_\alpha x^\alpha}$$

and

$$\Psi_{\mu\nu} = \varepsilon_{\mu\nu} e^{iq_\alpha x^\alpha} + \varepsilon_{\mu\nu}^* e^{-iq_\alpha x^\alpha},$$

where $k_\alpha k^\alpha = 0$ and $q_\alpha q^\alpha = -m_\Psi^2$. Substituting this last result and Eq. (22) in the transformation (21) we get

$$\begin{aligned} \varepsilon'_{\mu\nu} &= \varepsilon_{\mu\nu}, \\ \tilde{\varepsilon}'_{\mu\nu} &= \tilde{\varepsilon}_{\mu\nu} + k_\mu b_\nu + k_\nu b_\mu - \eta_{\mu\nu} k^\beta b_\beta. \end{aligned} \quad (23)$$

we get

$$\begin{aligned} \Psi_{00} &= -\frac{q^2}{m_\Psi^2} \Psi_D, \quad \Psi_{01} = \frac{q}{\omega_q} \Psi_B, \quad \Psi_{02} = \frac{q}{\omega_q} \Psi_C, \quad \Psi_{03} = \frac{q\omega_q}{m_\Psi^2} \Psi_D, \quad \Psi_{33} = -\frac{\omega_q^2}{m_\Psi^2} \Psi_D, \\ \Psi_{11} &= \frac{1}{2} \Psi_D + \Psi_+ \quad \text{and} \quad \Psi_{22} = \frac{1}{2} \Psi_D - \Psi_+. \end{aligned}$$

Therefore, in matrix form, we have

$$\begin{aligned} \Psi_{\mu\nu} &= \Psi_+ \begin{pmatrix} 0 & 0 & 0 & 0 \\ 0 & 1 & 0 & 0 \\ 0 & 0 & -1 & 0 \\ 0 & 0 & 0 & 0 \end{pmatrix} + \Psi_\times \begin{pmatrix} 0 & 0 & 0 & 0 \\ 0 & 0 & 1 & 0 \\ 0 & 1 & 0 & 0 \\ 0 & 0 & 0 & 0 \end{pmatrix} + \Psi_B \begin{pmatrix} 0 & \frac{q}{\omega_q} & 0 & 0 \\ \frac{q}{\omega_q} & 0 & 0 & -1 \\ 0 & 0 & 0 & 0 \\ 0 & -1 & 0 & 0 \end{pmatrix} + \Psi_C \begin{pmatrix} 0 & 0 & \frac{q}{\omega_q} & 0 \\ 0 & 0 & 0 & 0 \\ \frac{q}{\omega_q} & 0 & 0 & -1 \\ 0 & 0 & -1 & 0 \end{pmatrix} \\ &+ \Psi_D \begin{pmatrix} -\frac{q^2}{m_\Psi^2} & 0 & 0 & \frac{q\omega_q}{m_\Psi^2} \\ 0 & \frac{1}{2} & 0 & 0 \\ 0 & 0 & \frac{1}{2} & 0 \\ \frac{q\omega_q}{m_\Psi^2} & 0 & 0 & -\frac{\omega_q^2}{m_\Psi^2} \end{pmatrix}, \end{aligned}$$

where Ψ_+ , Ψ_\times , Ψ_B , Ψ_C and Ψ_D correspond to the 5 degrees of freedom of $\Psi_{\mu\nu}$.

III. SOLUTIONS TO THE LINEARIZED FIELD EQUATIONS

The physical solution of Eq. (14) is well known and given by

$$\tilde{h}_{\mu\nu}(t_r, \mathbf{x}) = \frac{\kappa}{2\pi} \int d^3x' \frac{1}{|\mathbf{x} - \mathbf{x}'|} T_{\mu\nu}(t_r, \mathbf{x}'),$$

where $t_r = t - \frac{|\mathbf{x} - \mathbf{x}'|}{c}$ is the retarded time and \mathbf{x} (the vector \mathbf{x}') points from the origin of the coordinate system

Based on Eqs. (19) and (23), we conclude that the massless spin-2 mode has only 2 degrees of freedom as in general relativity. Furthermore, for the vacuum solution, we can choose the traceless-transverse gauge where $\tilde{h}_{\mu 0} = 0$, $\partial^i \tilde{h}_{ij} = 0$ and $\tilde{h}^i_i = 0$. The massive spin-2 mode has 5 degrees of freedom since $\partial^\mu \Psi_{\mu\nu} = 0$ and $\Psi = 3\phi$. Considering the vacuum solution we can choose $\phi = \Psi/3 = 0$.

For completeness, it is interesting to explicitly determine the 5 degrees of freedom of $\Psi_{\mu\nu}$ for a monochromatic wave propagating in the z-direction [53]. In this case,

$$q^\mu = (\omega_q, 0, 0, q) \quad \text{and} \quad \omega_q^2 = q^2 + m_\Psi^2.$$

Using the gauge conditions $\partial^\mu \Psi_{\mu\nu} = 0$, $\Psi = 0$ and defining

$$\begin{aligned} \Psi_+ &= \frac{\Psi_{11} - \Psi_{22}}{2}, \quad \Psi_D = \Psi_{11} + \Psi_{22}, \\ \Psi_\times &= \Psi_{12}, \quad \Psi_B = -\Psi_{13} \quad \text{and} \quad \Psi_C = -\Psi_{23} \end{aligned} \quad (24)$$

to the observer (to the source). The formal solutions to the equations (18) and (9) are given by

$$\Phi(\mathbf{x}, t) = -\frac{\kappa}{3} \int G_\Phi(x^\mu; x'^\mu) T(t', \mathbf{x}') d^4x', \quad (25)$$

$$\Psi_{\mu\nu}(\mathbf{x}, t) = 2\kappa \int G_\Psi(x^\mu; x'^\mu) T_{\mu\nu}(t', \mathbf{x}') d^4x'. \quad (26)$$

The retarded Green's functions that appear in the previous equations are described by the expression

$$G_X(x^\mu; x'^\mu) = -\frac{1}{4\pi} \frac{1}{c} \frac{1}{s} \delta\left(\tau - \frac{s}{c}\right) + \frac{1}{4\pi} \frac{1}{c} \frac{m_X}{\sqrt{\tau^2 - \left(\frac{s}{c}\right)^2}} J_1\left(m_X c \sqrt{\tau^2 - \left(\frac{s}{c}\right)^2}\right) \Theta\left(\tau - \frac{s}{c}\right), \quad (27)$$

where $\tau = t - t'$, $s = |\mathbf{s}| = |\mathbf{x} - \mathbf{x}'|$, and X represents Φ or Ψ . The function Θ is the Heaviside step function and J_1 is the Bessel function of the first kind. Details on the deduction of Eq. (27) can be seen in Appendix A of Ref. [45].

Substituting Green's function in Eqs. (25) and (26) and considering large distances from the source, i.e. $s \simeq |\mathbf{x}| \equiv r$, we get

$$\Phi(\mathbf{x}, t) = \frac{\kappa}{12\pi} \frac{1}{r} \int T(\mathbf{x}', t_r) d^3\mathbf{x}' - \frac{m_\Phi}{12\pi} \kappa \int d^3\mathbf{x}' \int_{\frac{r}{c}}^{\infty} d\bar{t} \frac{J_1\left(m_\Phi c \sqrt{\bar{t}^2 - \left(\frac{r}{c}\right)^2}\right)}{\sqrt{\bar{t}^2 - \left(\frac{r}{c}\right)^2}} T(\mathbf{x}', t - \bar{t}) \quad (28)$$

and

$$\Psi_{ij}(\mathbf{x}, t) = -\frac{\kappa}{2\pi r} \int d^3\mathbf{x}' T_{ij}(\mathbf{x}', t_r) + \frac{m_\Psi}{2\pi} \kappa \int d^3\mathbf{x}' \int_{\frac{r}{c}}^{\infty} d\bar{t} \frac{J_1\left(m_\Psi c \sqrt{\bar{t}^2 - \left(\frac{r}{c}\right)^2}\right)}{\sqrt{\bar{t}^2 - \left(\frac{r}{c}\right)^2}} T_{ij}(\mathbf{x}', t - \bar{t}). \quad (29)$$

Note that by the degrees of freedom of $\Psi_{\mu\nu}$ it is enough to calculate its spatial components. See Sec. II A.

The next step is to perform the multipolar expansion for the fields $h_{\mu\nu}$, Φ and Ψ_{ij} . The multipolar expansion for the massless spin-2 field is well known from GR. The

expansion procedure for the scalar field was deduced in Ref. [45] and results in

$$\Phi(\mathbf{x}, t) = \Phi^M(\mathbf{x}, t) + \Phi^D(\mathbf{x}, t) + \Phi^Q(\mathbf{x}, t) + \dots,$$

where the monopole (M), dipole (D), and quadrupole (Q) contributions are given by

$$\Phi^M(\mathbf{x}, t) = \frac{\kappa}{12\pi r} [c^2 \mathcal{M}(t_r)] - \frac{m_\Phi}{12\pi} \kappa \int_0^\infty d\bar{t}_r F_\Phi(\bar{t}_r) [c^2 \mathcal{M}(\zeta)], \quad (30)$$

$$\Phi^D(\mathbf{x}, t) = \frac{\kappa}{12\pi r} \left[cn_i \frac{\partial \mathcal{M}^i}{\partial t} \Big|_{t_r} \right] - \frac{m_\Phi}{12\pi} \kappa \int_0^\infty d\bar{t}_r F_\Phi(\bar{t}_r) \left[cn_i \frac{\partial \mathcal{M}^i}{\partial t} \Big|_{\zeta} \right], \quad (31)$$

$$\Phi^Q(\mathbf{x}, t) = \frac{\kappa}{12\pi r} \left[\frac{1}{2} n_i n_j \frac{\partial^2 \mathcal{M}^{ij}}{\partial t^2} \Big|_{t_r} \right] - \frac{m_\Phi}{12\pi} \kappa \int_0^\infty d\bar{t}_r F_\Phi(\bar{t}_r) \left[\frac{1}{2} n_i n_j \frac{\partial^2 \mathcal{M}^{ij}}{\partial t^2} \Big|_{\zeta} \right], \quad (32)$$

with the unit vector n^i pointing along the x^i direction, $\zeta = t_r - \bar{t}_r$ and

$$F_\Phi(\bar{t}_r) = \frac{J_1\left(m_\Phi c \sqrt{2\bar{t}_r} \sqrt{\frac{\bar{t}_r}{2} + \frac{r}{c}}\right)}{\sqrt{2\bar{t}_r} \sqrt{\frac{\bar{t}_r}{2} + \frac{r}{c}}}. \quad (33)$$

The mass moments built with the trace of the energy-

momentum tensor are defined as

$$\mathcal{M}(t) \equiv \frac{1}{c^2} \int d^3\mathbf{x}' T(\mathbf{x}', t), \quad (34)$$

$$\mathcal{M}^i(t) \equiv \frac{1}{c^2} \int d^3\mathbf{x}' T(\mathbf{x}', t) x'^i, \quad (35)$$

$$\mathcal{M}^{ij}(t) \equiv \frac{1}{c^2} \int d^3\mathbf{x}' T(\mathbf{x}', t) x'^i x'^j. \quad (36)$$

The multipolar expansion for the massive spin-2 field follows similar steps to those performed for the Φ field. Thus, we get

$$\Psi_{ij}(\mathbf{x}, t) = \frac{\kappa}{2\pi} \left[-\frac{1}{r} S_{ij}(t_r) + m_\Psi \int_0^\infty d\bar{t}_r F_\Psi(\bar{t}_r) S_{ij}(\zeta) - \frac{1}{r} \frac{n_k}{c} \frac{\partial S^{ij,k}}{\partial t} \Big|_{t_r} + m_\Psi \int_0^\infty d\bar{t}_r F_\Psi(\bar{t}_r) \frac{n_k}{c} \frac{\partial S^{ij,k}}{\partial t} \Big|_\zeta + \dots \right],$$

where $F_\Psi(\bar{t}_r)$ is given by Eq. (33) switching $m_\Phi \rightarrow m_\Psi$. The first two moments of the stress tensor T^{ij} are defined as

$$S^{ij}(t) \equiv \int d^3\mathbf{x}' T^{ij}(\mathbf{x}', t)$$

and

$$S^{ij,k}(t) \equiv \int d^3\mathbf{x}' T^{ij}(\mathbf{x}', t) x^k.$$

Furthermore, the first moment S^{ij} can be written as $S^{ij} = \frac{1}{2} \dot{M}^{ij}$, where

$$M^{ij} = \frac{1}{c^2} \int d^3\mathbf{x}' T^{00}(\mathbf{x}', t) x'^i x'^j \quad (37)$$

is the usual quadrupole mass moment of general relativity.

Therefore, using the traceless-transverse (TT) gauge for $\tilde{h}_{\mu\nu}$ and taking into account only the dominant terms of each mode, we have

$$[\tilde{h}_{ij}^{TT}(\mathbf{x}, t)]_Q = \frac{1}{r} \frac{\kappa}{4\pi} \Lambda_{ij,kl}(\hat{\mathbf{n}}) \ddot{M}^{kl}(t_r), \quad (38)$$

$$[\Psi_{ij}(\mathbf{x}, t)]_Q = -\frac{1}{r} \frac{\kappa}{4\pi} \ddot{M}_{ij}(t_r) + \frac{\kappa}{4\pi} m_\Psi \int_0^\infty d\bar{t}_r F_\Psi(\bar{t}_r) \ddot{M}_{ij}(\zeta), \quad (39)$$

$$\Phi(\mathbf{x}, t) = \Phi^M(\mathbf{x}, t) + \Phi^D(\mathbf{x}, t) + \Phi^Q(\mathbf{x}, t), \quad (40)$$

where $\Lambda_{ij,kl}$ is a projection tensor that selects the TT gauge [54]. We will see in the next section that for a binary system with nonrelativistic dynamics $\Phi^M = \Phi^D = 0$, and thus the dominant term of the scalar part will also be a quadrupole term.

IV. BINARY SYSTEM IN CIRCULAR ORBIT

We begin by writing the energy-momentum tensor for a nonrelativistic binary point-mass system m_A in the center-of-mass frame:

$$T_{\mu\nu} = \sum_{A=1}^2 m_A c^2 \delta_\mu^0 \delta_\nu^0 \delta^{(3)}(\mathbf{x} - \mathbf{x}_A(t)),$$

where $\mathbf{x}_A(t)$ is the vector representing the trajectory of particle A . From this energy-momentum tensor and its

trace, we can calculate the mass moments for spin-0 and spin-2 modes in the center-of-mass ($c.m.$) frame. So, by Eqs. (34), (35), (36), and (37) we get

$$\begin{aligned} \mathcal{M}(t) &= -m, \quad \mathcal{M}^i(t) = 0 \quad \text{and} \\ \mathcal{M}^{ij}(t) &= -\mu x_0^i(t) x_0^j(t) = -M^{ij}(t), \end{aligned} \quad (41)$$

where $m = m_1 + m_2$ is the total mass, $\mu = m_1 m_2 / m$ is the reduced mass and $x_0^i(t)$ is the relative coordinate $\mathbf{x}_0 = \mathbf{x}_1 - \mathbf{x}_2$. The above expression shows that the monopole and dipole contributions to the spin-0 mode are zero. This result reflects the conservation of mass and linear momentum of a nonrelativistic binary system.

The next step is to determine the trajectory $x_0^i(t)$. For simplicity, we will consider a circular orbit of radius R and angular frequency ω_s positioned along the XY-plane. In this case, the relative coordinate is given by

$$x_0^i(t) = \left(R \cos\left(\omega_s t + \frac{\pi}{2}\right), R \sin\left(\omega_s t + \frac{\pi}{2}\right), 0 \right), \quad (42)$$

and the unit vector $n_{CM}^i = (0, 0, 1)$. Note that as the orbit is restricted to the XY-plane, the mass moments $M^{13} = M^{23} = M^{33} = 0$, which implies $\Psi_B = \Psi_C = \Psi_D = 0$. Thus, of the 5 degrees of freedom associated with Ψ_{ij} , only the transverse modes Ψ_+ and Ψ_- are produced.

By fixing the coordinate system at the observer's point of view, we can decompose the unit vector n^i in terms of the polar angle θ and the azimuthal angle ϕ as

$$n^i = (\sin \theta \sin \phi, \sin \theta \cos \phi, \cos \theta).$$

In this reference frame, ϕ represents a phase in the XY-plane, and θ is the angle between the normal of the orbit plane and the line of sight. For more details, see Figs. 3.2 and 3.6 of Ref. [54].

The spin-0, massive spin-2, and massless spin-2 modes are obtained by substituting the moments M^{ij} and \mathcal{M}^{ij} present in (41) in Eqs. (38), (39), (40), and (32), and then calculating the integrals that contain the functions F_Ψ and F_Φ . The calculation of these integrals is not trivial and can be found in Appendix B of Ref. [45]. Carrying out all these calculations, considering the chirp mass $M_c \equiv m^{\frac{2}{5}} \mu^{\frac{3}{5}}$ and the Kepler's third law $\omega_s^2 = Gm/R^3$, we obtain

$$\tilde{h}_+(\mathbf{x}, t) = \frac{4c}{r} \left(\frac{GM_c}{c^3} \right)^{\frac{5}{3}} \omega_s^{2/3} \left(\frac{1 + \cos^2 \theta}{2} \right) \cos \left[2\omega_s \left(t - \frac{r}{c} \right) + 2\phi \right], \quad (43)$$

$$\tilde{h}_\times(\mathbf{x}, t) = \frac{4c}{r} \left(\frac{GM_c}{c^3} \right)^{\frac{5}{3}} \omega_s^{2/3} \cos \theta \sin \left[2\omega_s \left(t - \frac{r}{c} \right) + 2\phi \right], \quad (44)$$

for massless tensorial modes,

$$\Psi_+(\mathbf{x}, t) = \begin{cases} -\frac{4c}{r} \left(\frac{GM_c}{c^3} \right)^{\frac{5}{3}} \omega_s^{2/3} \left(\frac{1 + \cos^2 \theta}{2} \right) \cos(2\omega_s t + 2\phi) \exp \left[-m_\Psi r \sqrt{1 - \left(\frac{2\omega_s}{m_\Psi c} \right)^2} \right], & 2\omega_s < m_\Psi c \\ -\frac{4c}{r} \left(\frac{GM_c}{c^3} \right)^{\frac{5}{3}} \omega_s^{2/3} \left(\frac{1 + \cos^2 \theta}{2} \right) \cos \left[2\omega_s \left(t - \left(\frac{r}{c} \right) \sqrt{1 - \left(\frac{m_\Psi c}{2\omega_s} \right)^2} \right) + 2\phi \right], & 2\omega_s > m_\Psi c \end{cases}, \quad (45)$$

$$\Psi_\times(\mathbf{x}, t) = \begin{cases} -\frac{4c}{r} \left(\frac{GM_c}{c^3} \right)^{\frac{5}{3}} \omega_s^{2/3} \cos \theta \sin(2\omega_s t + 2\phi) \exp \left[-m_\Psi r \sqrt{1 - \left(\frac{2\omega_s}{m_\Psi c} \right)^2} \right], & 2\omega_s < m_\Psi c \\ -\frac{4c}{r} \left(\frac{GM_c}{c^3} \right)^{\frac{5}{3}} \omega_s^{2/3} \cos \theta \sin \left[2\omega_s \left(t - \left(\frac{r}{c} \right) \sqrt{1 - \left(\frac{m_\Psi c}{2\omega_s} \right)^2} \right) + 2\phi \right], & 2\omega_s > m_\Psi c \end{cases}, \quad (46)$$

for the massive tensorial modes and

$$\Phi(\mathbf{x}, t) = \begin{cases} \frac{2c}{3r} \left(\frac{GM_c}{c^3} \right)^{\frac{5}{3}} \omega_s^{2/3} \sin^2 \theta \cos(2\omega_s t + 2\phi) \exp \left[-m_\Phi r \sqrt{1 - \left(\frac{2\omega_s}{m_\Phi c} \right)^2} \right], & 2\omega_s < m_\Phi c \\ \frac{2c}{3r} \left(\frac{GM_c}{c^3} \right)^{\frac{5}{3}} \omega_s^{2/3} \sin^2 \theta \cos \left[2\omega_s \left(t - \left(\frac{r}{c} \right) \sqrt{1 - \left(\frac{m_\Phi c}{2\omega_s} \right)^2} \right) + 2\phi \right], & 2\omega_s > m_\Phi c \end{cases}, \quad (47)$$

for massive scalar mode.

The most relevant point of the solutions above is that the massive modes have two distinct regimes. The first of these is a damping regime that occurs when $2\omega_s < m_\chi c$.⁸ In this regime we do not have a wave solution, and the massive modes only contribute with a temporal modulation for the gravitational field that exponentially decays when moving away from the source. The second regime, called the oscillatory regime, occurs when $2\omega_s > m_\chi c$. It is only in this regime that the source emits gravitational waves associated with the massive modes.

The solutions for \tilde{h}_+, Ψ_+ and $\tilde{h}_\times, \Psi_\times$ in the oscillatory regime are waves of the same amplitude, same frequency and different wave numbers, which provides an interpretation of interference effects. In this sense, it is convenient to introduce

$$\Theta_{+,\times} = \tilde{h}_{+,\times} + \Psi_{+,\times}. \quad (48)$$

Equation (48) allows us to interpret the spin-2 waves as a single structure generated by interference between the

fields $\tilde{h}_{+,\times}$ and $\Psi_{+,\times}$. Note that due to the difference in sign between $\tilde{h}_{+,\times}$ and $\Psi_{+,\times}$, what we have is a destructive interference effect. Furthermore, at the limit of $m_\Psi \rightarrow 0$, this destructive interference is complete, and in this case, the emission of tensorial modes does not occur. We will see in the next sections that physical interpretations of the binary system are consistent only when we treat massive and massless spin-2 modes together.

A. Gravitational energy-momentum tensor and the power radiated

The low-frequency effects of second-order terms contribute to background changes [6]. These terms, obtained from space-time averages $\langle \dots \rangle$, generate the gravitational energy-momentum tensor $t_{\mu\alpha}$ given by

$$t_{\mu\alpha} = -\frac{c^4}{8\pi G} \left[\left\langle G_{\mu\alpha}^{(2)} \right\rangle + \gamma \left\langle H_{\mu\alpha}^{(2)} \right\rangle - 2\alpha \left\langle I_{\mu\alpha}^{(2)} \right\rangle \right], \quad (49)$$

⁷ For certain configurations of the binary system, the circular orbit approximation can be quite realistic if we assume that the process of circularization of elliptical orbits of general relativity

also occurs in quadratic gravity. The study of circularization in quadratic gravitation will be carried out in a future work.

⁸ Remembering that X represents Φ or Ψ .

where

$$G_{\mu\alpha}^{(2)} = R_{\mu\alpha}^{(2)} - \frac{1}{2}\eta_{\mu\alpha}R^{(2)} - \frac{1}{2}h_{\mu\alpha}R^{(1)}, \quad (50)$$

$$H_{\mu\alpha}^{(2)} = R^{(1)}R_{\mu\alpha}^{(1)} - \frac{1}{4}R^{(1)}R^{(1)}\eta_{\mu\alpha} + h_{\mu\alpha}\partial^\sigma\partial_\sigma R^{(1)} + \eta_{\mu\alpha}\Box^{(1)}R^{(1)} + \eta_{\mu\alpha}\partial^\sigma\partial_\sigma R^{(2)} - \nabla_\mu^{(1)}\partial_\alpha R^{(1)} - \partial_\mu\partial_\alpha R^{(2)}, \quad (51)$$

$$I_{\mu\alpha}^{(2)} = (\nabla^\nu\nabla^\beta)^{(1)}C_{\mu\nu\alpha\beta}^{(1)} + \partial^\nu\partial^\beta C_{\mu\nu\alpha\beta}^{(2)} + \frac{1}{2}R^{\nu\beta(1)}C_{\mu\nu\alpha\beta}^{(1)}. \quad (52)$$

After a long calculation presented in Appendix A, we get

$$t_{\mu\alpha} = \frac{c^4}{8\pi G} \left[\frac{1}{4} \langle \partial_\mu \tilde{h}_{\nu\beta} \partial_\alpha \tilde{h}^{\nu\beta} \rangle - \frac{1}{4} \langle \partial_\mu \Psi_{\nu\beta} \partial_\alpha \Psi^{\nu\beta} \rangle + \frac{3}{2} \langle \partial_\alpha \Phi \partial_\mu \Phi \rangle + \frac{1}{2} \langle \partial_\mu \tilde{h}_{\nu\beta} \partial_\alpha \Psi^{\nu\beta} \rangle \right]. \quad (53)$$

An important point to be discussed is the opposite (negative) sign that appears in the second term of Eq. (53) [55]. Although potentially pathological, this negative sign is expected because the Weyl-Weyl term presents Ostrogradsky instability, implying that the Hamiltonian density is not positive definite.⁹ However, in the context we are studying, it is possible to avoid any pathology by considering the massive and massless spin-2 modes as a single structure defined in Eq. (48). In this context, neglecting the scalar mode, we have two different situations:

- For $2\omega_s < m_\Psi c$ (damping regime), the massive spin-2 part does not emit radiation – $\langle \partial_\mu \Psi_{\nu\beta} \partial_\alpha \Psi^{\nu\beta} \rangle = 0$ – and the system behaves as in general relativity.

- For $2\omega_s > m_\Psi c$ (oscillatory regime), spin-2 modes emit two waves that interfere destructively in such a way that the radiated energy is always less than the case of pure GR but always positive, i.e., $\langle \partial_\mu \tilde{h}_{\nu\beta} \partial_\alpha \tilde{h}^{\nu\beta} \rangle - \langle \partial_\mu \Psi_{\nu\beta} \partial_\alpha \Psi^{\nu\beta} \rangle > 0$.

The radiated power per solid angle unit is given by

$$\frac{dP}{d\Omega} = -cr^2 t_{01}. \quad (54)$$

Due to the functional form of $\tilde{h}_{+,\times}$ their radial derivatives ∂_1 can be switched to time derivatives ∂_0 up to $\mathcal{O}(1/r^2)$:

$$\partial_1 \tilde{h}_{+,\times} = -\partial_0 \tilde{h}_{+,\times}.$$

Furthermore, using analogous reasoning for $\Psi_{+,\times}$ and Φ , we obtain

$$\begin{aligned} \partial_1 \Psi_+ &= \begin{cases} \sqrt{\left(\frac{m_\Psi c}{2\omega_s}\right)^2 - 1} \cot(2\omega_s t + 2\phi) \partial_0 \Psi_+, & 2\omega_s < m_\Psi c \\ -\sqrt{1 - \left(\frac{m_\Psi c}{2\omega_s}\right)^2} \partial_0 \Psi_+, & 2\omega_s > m_\Psi c \end{cases}, \\ \partial_1 \Psi_\times &= \begin{cases} -\sqrt{\left(\frac{m_\Psi c}{2\omega_s}\right)^2 - 1} \tan(2\omega_s t + 2\phi) \partial_0 \Psi_\times, & 2\omega_s < m_\Psi c \\ -\sqrt{1 - \left(\frac{m_\Psi c}{2\omega_s}\right)^2} \partial_0 \Psi_\times, & 2\omega_s > m_\Psi c \end{cases} \end{aligned}$$

and

$$\partial_1 \Phi = \begin{cases} \sqrt{\left(\frac{m_\Phi c}{2\omega_s}\right)^2 - 1} \cot(2\omega_s t + 2\phi) \partial_0 \Phi, & 2\omega_s < m_\Phi c \\ -\sqrt{1 - \left(\frac{m_\Phi c}{2\omega_s}\right)^2} \partial_0 \Phi, & 2\omega_s > m_\Phi c \end{cases}.$$

⁹ This phenomenon has been known for a long time in the context of quadratic gravity quantization [47].

Substituting these last results in Eq. (54) and calculating the spatial-time averages, we get [45]

$$\begin{aligned} \frac{dP}{d\Omega} = & -\frac{2G\mu^2 R^4 \omega_s^6}{\pi c^5} \left[\left(\left(\frac{1 + \cos^2 \theta}{2} \right)^2 + \cos^2 \theta \right) \left(1 - \Theta(2\omega_s - m_\Psi c) \sqrt{1 - \left(\frac{m_\Psi c}{2\omega_s} \right)^2} \right) \right. \\ & \left. + \Theta(2\omega_s - m_\Phi c) \sqrt{1 - \left(\frac{m_\Phi c}{2\omega_s} \right)^2} \frac{1}{12} \sin^4 \theta \right]. \end{aligned} \quad (55)$$

The Heaviside functions $\Theta(2\omega_s - m_\Psi c)$ and $\Theta(2\omega_s - m_\Phi c)$ indicate that only the oscillatory regimes contribute to the radiated power. It is also worth noting that the cross term $\langle \partial_0 \tilde{h}_{\nu\beta} \partial_1 \Psi^{\nu\beta} \rangle$ cancels out when averaged in time and space. One additional integration gives the expression for the total power radiated:

$$P = -\frac{32}{5} \frac{c^5}{G} \left(\frac{GM_c \omega_s}{c^3} \right)^{\frac{10}{3}} \left[1 - \Theta(2\omega_s - m_\Psi c) \sqrt{1 - \left(\frac{m_\Psi c}{2\omega_s} \right)^2} + \frac{\Theta(2\omega_s - m_\Phi c)}{18} \sqrt{1 - \left(\frac{m_\Phi c}{2\omega_s} \right)^2} \right]. \quad (56)$$

Considering the tensorial part in the oscillatory regime and the scalar part in the damping regime, we get

$$P_{spin2} = -\frac{32}{5} \frac{c^5}{G} \left(\frac{GM_c \omega_s}{c^3} \right)^{\frac{10}{3}} \left[1 - \sqrt{1 - \left(\frac{m_\Psi c}{2\omega_s} \right)^2} \right].$$

This last expression corroborates the previous statement that the emitted energy is always positive definite. In fact, for $m_\Psi c = 2\omega_s$, we are at the threshold of the damping regime and the system loses energy exclusively by the massless spin-2 mode. As m_Ψ decreases, the destructive interference effect occurs between $\tilde{h}_{+, \times}$ and $\Psi_{+, \times}$ and the energy loss decreases monotonically. In the limiting case where $m_\Psi \rightarrow 0$, the destructive interference is maximum and the energy loss ceases to exist via tensorial modes. It is worth remembering that the limit $m_\Psi \rightarrow 0 \Rightarrow \alpha \rightarrow \infty$ is nonphysical since the term $C_{\mu\nu\alpha\beta} C^{\mu\nu\alpha\beta}$ diverges in the action (1).

V. INSPIRAL PHASE OF BINARY BLACK HOLES

Let us consider the case of a binary system consisting of two static black holes with spherical symmetry. For simplicity, we will adopt the Schwarzschild solution as a static solution, although, in quadratic gravity, other solutions might exist [56, 57]. Thus, in the weak field regime, the gravitational potential is reduced to the Newtonian potential.

The next step is to establish the balance equation that determines the energy loss of the system through the emission of gravitational waves:

$$P = -\frac{dE_{orbit}}{dt}, \quad (57)$$

where P is the total radiated power and

$$\frac{dE_{orbit}}{dt} = \frac{Gm_1 m_2}{2R^2} \dot{R}, \quad (58)$$

is obtained in the approximation of quasicircular orbits [54]. Substituting Eqs. (56) and (58) in the expression (57) and using Kepler's third law, we get

$$\dot{\omega}_s = \frac{96}{5} \left(\frac{GM_c}{c^3} \right)^{\frac{5}{3}} \omega_s^{\frac{11}{3}} \left\{ 1 - \Theta(2\omega_s - m_\Psi c) \sqrt{1 - \left(\frac{m_\Psi c}{2\omega_s} \right)^2} + \frac{\Theta(2\omega_s - m_\Phi c)}{18} \sqrt{1 - \left(\frac{m_\Phi c}{2\omega_s} \right)^2} \right\}. \quad (59)$$

The equation (59) determines the variation of the orbital frequency in the inspiral phase. The term within curly brackets contains the usual contribution from GR (first term) and additional contributions from the massive spin-2 and spin-0 modes. The massive modes only contribute when $\Theta(2\omega_s - m_\Psi c) = 1$ or $\Theta(2\omega_s - m_\Phi c) = 1$,

that is, only when the solutions are in the oscillatory regime.

To analyze the effect of massive modes in the binary system, we will divide the study into two cases: in the first one, we only consider the tensorial mode in the oscillatory regime; in the second, we only take into account

the scalar mode.

GR plus massive spin-2 mode: In this case we have $2\omega_s > m_\Psi c$ and $2\omega_s < m_\Phi c$, so that Eq. (59) contains only the first two terms. By integrating Eq. (59), we get the curves shown in Fig. 1:

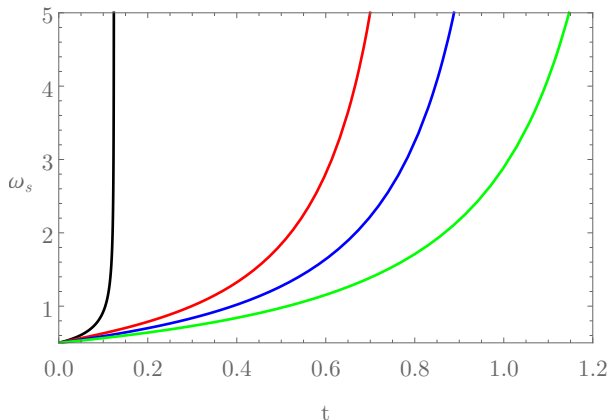


FIG. 1. Numerical solution of the balance equation in units of $GM_c/c^3 = 1$, with initial condition $\omega(0) = 0.5$ and taking into account only spin-2 modes. The red, blue and green curves are constructed with $m_\Psi c = 1$, $m_\Psi c = 0.9$ and $m_\Psi c = 0.8$, respectively. The black curve represents the pure GR solution.

Figure 1 presents solutions for the combined spin-2 structure, i.e. $\Theta_{\mu\nu} = \tilde{h}_{\mu\nu} + \Psi_{\mu\nu}$, and the pure case of general relativity. This figure clearly shows that the coalescence time increases as the value $m_\Psi c$ decreases. It occurs because the reduction of $m_\Psi c$ makes the process of destructive interference between the $\tilde{h}_{\mu\nu}$ and $\Psi_{\mu\nu}$ modes more effective, and consequently, the binary system loses energy more slowly. It is important to note that for $m_\Psi c > 0$, i.e. α finite, coalescence always occurs.

GR plus massive spin-0 mode: In this other configuration we have $2\omega_s < m_\Psi c$ and $2\omega_s > m_\Phi c$, and therefore only the first and third terms are present in equation (59). By integrating Eq. (59) in this context, we get the results shown in Fig. 2.

Figure 2 presents $\omega_s(t)$ in the inspiral phase considering that the binary system loses energy through the $\tilde{h}_{\mu\nu}$ and Φ modes. From this figure, we can see that the lower the value of $m_\Phi c$, the more effective is the energy loss via scalar mode, and consequently, the coalescence occurs earlier. Furthermore, the proximity of the curves in Fig. 2 indicates that the scalar mode carries considerably less energy than the tensorial one, i.e. the orbital dynamics of the system is essentially determined by the $\tilde{h}_{\mu\nu}$ mode.

VI. SPIN-2 WAVEFORM

Once the orbital dynamics of the binary system is established, we will study what is the waveform of the unique spin-2 structure detected at a certain point in

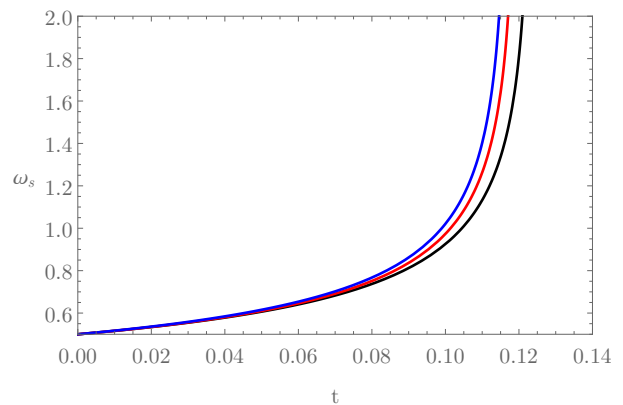


FIG. 2. Numerical solution of the balance equation in units of $GM_c/c^3 = 1$, with initial condition $\omega(0) = 0.5$ and taking into account only the spin-0 and massless spin-2 modes. The red and blue curves are constructed with $m_\Phi c = 1$ and $m_\Phi c = 0.1$, respectively. The black curve represents the pure general relativity solution.

space.¹⁰ We saw earlier that the complete spin-2 wave is composed of two modes, namely $\tilde{h}_{+,\times}$ and $\Psi_{+,\times}$, which interfere destructively. At the time of emission, these two modes have the same frequency and amplitude, but this is no longer true at the time of detection. The main point of this analysis is that the massive and massless modes propagate at different velocities. While the $\tilde{h}_{+,\times}$ mode propagates with velocity c , the $\Psi_{+,\times}$ mode propagates with group velocity

$$v_g(t) = \frac{d\omega}{dk},$$

where $\omega = c\sqrt{k^2 + m_\Psi^2}$ is the dispersion relation of the massive mode. Remembering that in the approximation of quasicircular orbits we have $\omega = 2\omega_s$, we can write the velocity v_g as

$$v_g = c\sqrt{1 - \left(\frac{m_\Psi c}{2\omega_s}\right)^2}, \quad (60)$$

with $v_g < c$. The difference in propagation velocities between the two modes generates the phenomenon of dispersion in the complete spin-2 wave.

The combination of massive and massless modes at detection time t_d occurs with waves that were emitted at different times and therefore have different frequencies. If the $\tilde{h}_{+,\times}$ mode was emitted in t_e , the $\Psi_{+,\times}$ mode was necessarily emitted earlier in t_{em} . In this case, the frequency $\omega_s(t_e)$ associated with the massless mode is greater than the frequency $\omega_s(t_{em})$ associated with the massive mode.

¹⁰ During this section, we assume that there is no scalar mode emission.

Based on the previous discussion, we can write the relationships between the detection time and the emission times as

$$t_e = t_d - \frac{r}{c}, \quad (61)$$

$$t_{em} = t_d - \frac{r}{v_g(t_{em})}. \quad (62)$$

Combining these two expressions and using Eq. (60), we get

$$t_{em} = t_e + \frac{r}{c} \left(1 - \frac{1}{\sqrt{1 - \left(\frac{m_{\Psi} c}{2\omega_s(t_{em})} \right)^2}} \right). \quad (63)$$

The previous equation is an algebraic equation for t_{em} which together with Eq. (59) allows us to determine t_{em} and $\omega_s(t_{em})$.

In order to exemplify the phenomenon of dispersion in the spin-2 complete wave, we consider a hypothetical binary system of $M_c = 10M_\odot$ located at a distance of $10Kpc$. We also assume $m_{\Psi}c = 0.02 s^{-1}$ and neglect the scalar mode emission.¹¹ For convenience t_e is adopted as a time evolution variable and we consider $\omega_s(t_e = 0) = 0.01 Hz$. This initial condition causes the $\Psi_{+,\times}$ mode to transition from the damping regime to the oscillatory one exactly at $t_e = 0$.

The next step is to numerically solve the balance equation (59) obtaining $\omega_s(t)$, and then determine t_{em} by Eq. (63) considering different values of t_e . To facilitate this analysis, we define the functions

$$f(t_{em}) = t_{em}$$

and

$$g(t_{em}) = t_e + \frac{r}{c} \left(1 - \frac{1}{\sqrt{1 - \left(\frac{m_{\Psi} c}{2\omega_s(t_{em})} \right)^2}} \right).$$

Figure 3 shows plots of the functions $f(t_{em})$ and $g(t_{em})$ for three distinct values of t_e .

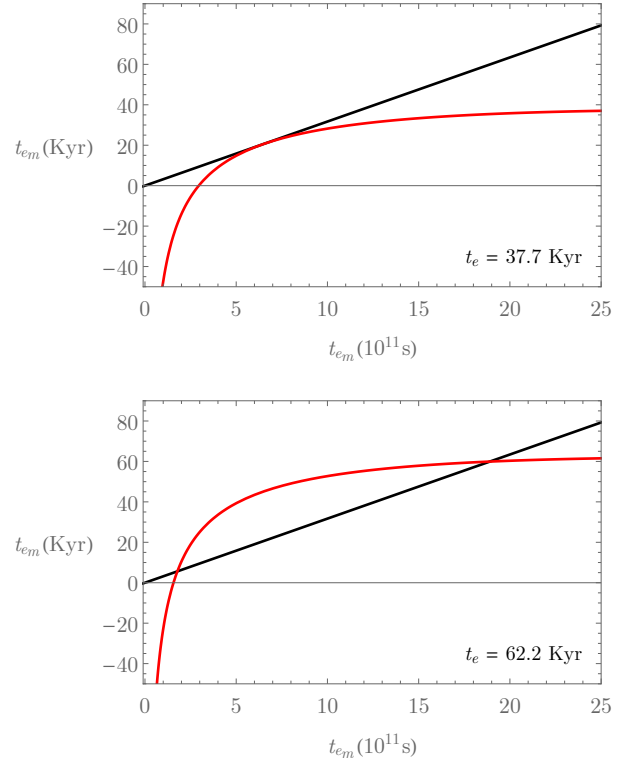
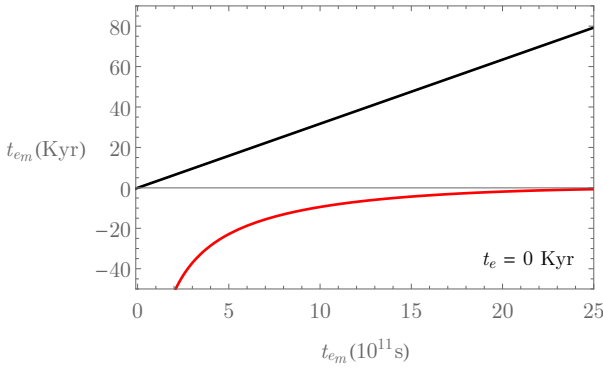


FIG. 3. Plots of the functions $f(t_{em})$ (black) and $g(t_{em})$ (red) considering three values of t_e . In the construction of $g(t_{em})$, we use the numerical solution of Eq. (59) with $M_c = 10M_\odot$, $r = 10 Kpc$, $m_{\Psi}c = 0.02 s^{-1}$ and initial condition $\omega_s(0) = 0.01 Hz$.

The plots sequence in Fig. 3 shows that as t_e increases, the red curve shifts upwards. Furthermore, from $t_e = 37.7 Kyr$, this curve intercepts the black curve indicating the existence of solutions of Eq. (63). Physically this means that the first wave fronts of the massive modes take $37.7 Kyr$ to travel a distance of $10 Kpc$. Furthermore, due to the nonlinearity of velocity $v_g(t)$, we see that the complete spin-2 wave detected is composed by the superposition of a massless mode $\tilde{h}_{+,\times}$ and two massive modes $\Psi_{+,\times}^{(1,2)}$. This fact is evidenced by the double solution of Eq. (63), which occurs from $t_e = 37.7 Kyr$. Figure 4 shows waveforms $\Theta_+ = \tilde{h}_+(\omega_s^e) + \Psi_+^{(1)}(\omega_s^{e_{m(1)}}) + \Psi_+^{(2)}(\omega_s^{e_{m(2)}})$ considering the same three values of t_e presented above.

The plots in Fig. 4 show the full tensorial mode waveforms associated with polarization plus. In the interval $0 \leq t_e < 37.7 Kyr$ only the massless mode is present, and Θ_+ has the form of a pure sinusoid. From $t_e \geq 37.7 Kyr$, the three modes \tilde{h}_+ , $\Psi_+^{(1)}$ and $\Psi_+^{(2)}$ combine and generate an interference pattern. For $t_e \approx 37.7 Kyr$ (second plot of figure 4), the two massive modes have similar frequencies and contribute similarly to the structure of Θ_+ . As t_e increases, the $\Psi_+^{(2)}$ mode (lower frequency mode) decreases in importance compared to $\Psi_+^{(1)}$. In the last plot of figure 4, we present a moment when the complete wave-

¹¹ This can be obtained by considering $m_{\Phi}c$ much higher than the typical orbital frequency of the binary system.

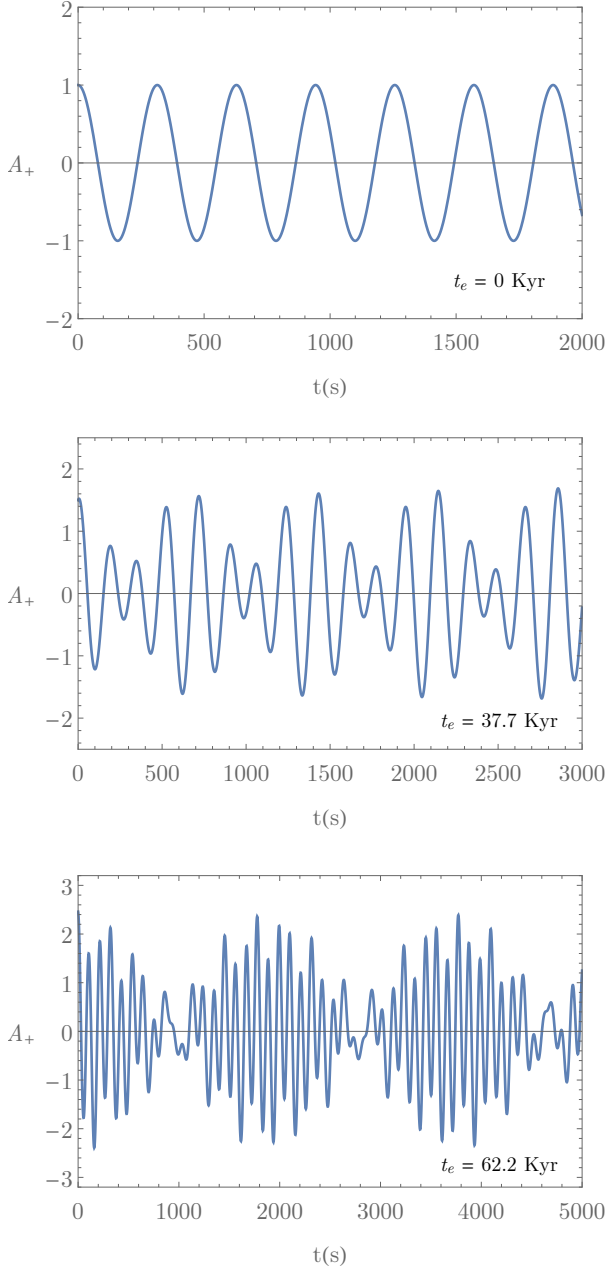


FIG. 4. Waveforms $\Theta_+ = \tilde{h}_+ + \Psi_+^{(1)} + \Psi_+^{(2)}$ normalized by the amplitude $A_+ = 2r^{-1}c^{-4} (GM_c)^{\frac{5}{3}} (1 + \cos^2 \theta) (\omega_s^e)^{\frac{2}{3}}$ associated with the \tilde{h}_+ mode. The first plot presents only the massless mode with frequency $\omega_s^e = 10^{-2} \text{ Hz}$. In the second plot, we have a massless frequency mode $\omega_s^e = 1.762 \times 10^{-2} \text{ Hz}$ and two massive frequency modes $\omega_s^{em(1)} = 1.326 \times 10^{-2} \text{ Hz}$ and $\omega_s^{em(2)} = 1.323 \times 10^{-2} \text{ Hz}$. In the third plot, the massless mode has frequency $\omega_s^e = 3 \times 10^{-2} \text{ Hz}$ and the two massive modes have frequencies $\omega_s^{em(1)} = 2.83 \times 10^{-2} \text{ Hz}$ and $\omega_s^{em(2)} = 1.07 \times 10^{-2} \text{ Hz}$. All frequencies were calculated from the solution of the balance equation (59).

form is mainly characterized by \tilde{h}_+ and $\Psi_+^{(1)}$, both with similar frequencies. In this case, we notice that Θ_+ is modulated by an angular frequency envelope $\omega_s^e - \omega_s^{em(1)}$

with some deformity generated by the presence of $\Psi_+^{(2)}$.

In the next section, we will use the nonexistence of an interference pattern in gravitational wave observations to constrain the parameter m_Ψ .

A. Observational constraints

The waveform detected in the inspiral phase of a binary black hole system allows constraining the parameter m_Ψ . It is possible because the presence of massive modes produces an interference pattern (plots in Fig. 4) that is clearly not observed. To obtain these constraints, we will consider the event GW170104, which consists of the merge of two black holes with a Chirp mass $M_c = 21.1 M_\odot$ and a distance of $r = 880 \text{ Mpc}$ [58].¹² Figure 1 of Ref. [58] indicates that the gravitational wave is detected initially at $t_{ini} = 0.5 \text{ s}$ with frequency $f_{GW} \approx 45 \text{ Hz}$, and the merge occurs around $t_{mer} = 0.59 \text{ s}$.

The estimated constraint for m_Ψ is performed as follows:

- Using the initial condition $\omega_s(t_{ini}) = \pi f_{GW} = 141 \text{ Hz}$, we numerically solve the balance equation (59) for different values of m_Ψ . It is done considering that the spin-0 mode is in the damping regime.
- Knowing $\omega_s(t)$ and using $t_e = t_{ini}$, we determine the largest value of m_Ψ in which Eq. (63) has a solution for t_{em} . Numerically this corresponds to a configuration equivalent to the second plot in Fig. 3.

The procedure above establishes the maximum value of m_Ψ at which the massive mode produces an interference pattern of the type shown in Fig. 4. As this pattern is not observed in event GW170104, the maximum value obtained establishes a lower bound for m_Ψ . Table I shows the result of this constraint:

	ω_s^e	ω_s^{em}	$m_\Psi (\gtrsim)$	$\alpha (\lesssim)$
Spin-2	141 Hz	77 Hz	$4.2 \times 10^{-11} m^{-1}$	$1.1 \times 10^{21} m^2$

TABLE I. Emission frequencies of the massive (ω_s^{em}) and massless (ω_s^e) tensorial modes, and constraints for the parameters m_Ψ and α where $m_\Psi^2 = 2/\alpha$. Note that the two massive modes have approximately the same frequency given by ω_s^{em} . Furthermore, since ω_s^e and ω_s^{em} differ only by a factor of 2, the amplitudes of the modes $\Psi_{+,\times}^{(1,2)}$ and $\tilde{h}_{+,\times}$ are similar. Thus, for $m_\Psi < 4.2 \times 10^{-11} m^{-1}$, we obtain an interference pattern similar to the one shown in the second plot of figure 4.

Another way to obtain a more restrictive constraint for m_Ψ is through the coalescence time Δ_{col} . From Fig. 1, we see that the coalescence time increases substantially

¹² We only take into account the best-fit parameters.

as $m_\Psi c$ decreases. On the other hand, event GW170104 observes a coalescence time $\Delta_{col}^{ob} \sim 0.1$ s counted from the initial setting $\omega_s(t_{ini}) = 141$ Hz. Thus, imposing that the presence of the massive mode cannot change (in order of magnitude) the observed value of Δ_{col}^{ob} , we can constrain the parameters m_Ψ and α .

The coalescence time is calculated from Eq. (59) and essentially depends on the parameters M_c and m_Ψ .¹³ Solutions to this equation show that as M_c and m_Ψ increase Δ_{col} decreases. In principle, any decrease in m_Ψ can be offset by an increase in M_c leaving Δ_{col} invariant. However, there is strong theoretical [59] and observational [60, 61] evidence that the mass of Chirp is "always" less than $100M_\odot$.¹⁴ Thus, assuming the maximum value $M_c = 100M_\odot$, we can establish a lower bound for m_Ψ requiring Δ_{col} to be compatible with the observed value Δ_{col}^{ob} .

In Fig. 5, we show the solution $\omega_s(t)$ for different values of the parameter m_Ψ with $M_c = 100M_\odot$:

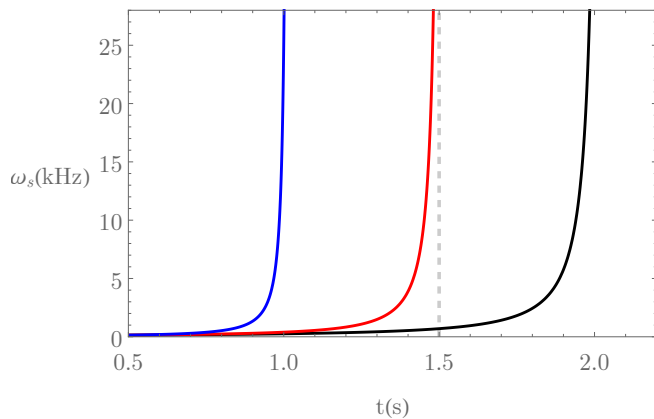


FIG. 5. Plot of the function $\omega_s(t)$ considering the initial condition $\omega_s(0.5) = 141$ Hz and $M_c = 100M_\odot$. The blue, red and black curves are constructed with $m_\Psi c = 120$ s⁻¹, $m_\Psi c = 86$ s⁻¹ and $m_\Psi c = 70$ s⁻¹, respectively. The vertical dashed curve indicates $\Delta_{col} = 1$ s.

The coalescence time is calculated from $\Delta_{col} = t_{col} - 0.5$, where t_{col} is the instant when the functions in Fig. 5 diverge. Thus, for the models described by the blue, red and black curves, we obtain $\Delta_{col} = 0.5$ s, 1 s and 1.5 s, respectively. Furthermore, these values correspond to the minimum coalescence times of a given model m_Ψ as they were calculated with the maximum value $M_c = 100M_\odot$. If we decrease the chirp mass with m_Ψ fixed, we get a larger value for Δ_{col} .

Based on the previous discussion, we can estimate a lower bound for the parameter m_Ψ considering $\Delta_{col} \leq \Delta_{col}^{ob}$. In principle, we should use $\Delta_{col}^{ob} \sim 0.1$ s. However,

to compensate for the errors generated by the approximations performed (nonrelativistic dynamics, point masses, etc.), we reduce the constraint by 1 order of magnitude and consider $\Delta_{col} \leq 1$ s.¹⁵ Thus, from Fig. 5, we see that $m_\Psi c$ must be larger than 86 s⁻¹, which results in the following constraint shown in Table II.

	$m_\Psi (\gtrsim)$	$\alpha (\gtrsim)$
Spin-2	$3 \times 10^{-7} m^{-1}$	$2 \times 10^{13} m^2$

TABLE II. Constraints to parameters m_Ψ and α taking into account $\Delta_{col} \leq 1$ s.

Due to the various approximations performed, the estimates presented in Table II must be considered only in order of magnitude. Still, the constraint for the α parameter via coalescence time is about 8 orders of magnitude more restrictive than the constraint obtained via the interference pattern.

VII. FINAL COMMENTS

In this paper, we studied GWs emitted by binary point-mass black hole systems in the context of the quadratic gravity model assuming nonrelativistic and circular orbit approximations. The GWs solutions were calculated by taking into account the dominant terms in the multipolar expansion. They exhibit three modes: a massive spin-2 mode $\Psi_{\mu\nu}$, a massive spin-0 mode Φ , and the expected massless spin-2 mode $\tilde{h}_{\mu\nu}$. Besides, the massive modes present two different behaviors: the oscillatory regime, which plays the real role of GW; and the damped regime, which presents an exponential decay.

We calculated the energy-momentum tensor $t_{\mu\nu}$ of the GWs and showed that it presents the Ostrogradsky instability. To circumvent this potential problem and obtain a consistent physical interpretation [62], we consider spin-2 waves as a single structure given as a result of the destructive interferences between the fields $\tilde{h}_{\mu\nu}$ and $\Psi_{\mu\nu}$. Having obtained the $t_{\mu\nu}$, we constructed the energy balance equation and studied how the quadratic gravity model modifies the orbital dynamics of point-mass black hole binaries. We showed that the spin-2 structure takes a longer time to reach coalescence indicating the system loses energy more slowly when compared to GR. For the case of spin-0 plus GR, we have a shorter time to reach coalescence indicating that the system loses energy faster than the GR pure case.

¹³ Again, we consider that the spin-0 mode is in the damping regime.

¹⁴ By "always" we mean that the existence of a binary black hole system with $M_c \gtrsim 100M_\odot$ is highly improbable.

¹⁵ Relativistic corrections are essential to correctly describe the orbital dynamics close to the merger. However, they do not change the coalescence time in order of magnitude. For example, the predicted coalescence time for event GW1701104 in GR on the quadrupole approximation is $\Delta_{col} = 0.16$ s.

We determined the waveform that a detector would observe for the complete spin-2 structure. When the massive mode is not present, we obtain a pure sine wave. However, when it is present, we get a clear interference pattern. Using the nonobservation of this interference pattern, we constrain the parameter to $m_\Psi \gtrsim 4.2 \times 10^{-11} m^{-1}$ or $\alpha \lesssim 1.1 \times 10^{21} m^2$. Furthermore, based on the coalescence time, we developed a second method to constrain m_Ψ . By this method, we obtain $m_\Psi \gtrsim 3 \times 10^{-7} m^{-1}$ or $\alpha \lesssim 2 \times 10^{13} m^2$, which is 8 orders of magnitude more restrictive than the previous one.

The methods presented in Sec. VIA do not effectively constrain the parameter m_Φ or γ . The main reason for this is the structural difference between the solutions Φ and $\Psi_{+, \times}$. For example, the scalar mode presents a longitudinal polarization differently from the tensor modes [63–65]. This difference leads to factor 1/18 which appears in the balance equation and makes the energy loss via scalar mode ineffective.

There are some papers in the literature that constrain the parameters of quadratic gravity. On astrophysical scales, of the order of stellar systems, we get restrictions associated with the scalar mode arising from binary systems. Using observations of decreasing orbital period of

neutron star binaries, Refs. [42, 66] and [45] constrain $\gamma \lesssim 10^{17} m^2$ and $\gamma \lesssim 10^{16} m^2$, respectively. At earthly scales, the Eöt-Wash torsion balance experiment [67] provides bounds for both γ and α parameters. Based on the static weak-field solution of quadratic gravity [47], the Eöt-Wash experiment constrains $\alpha \sim \gamma \lesssim 2 \times 10^{-9} m^2$. Even though earthly bounds are much more restrictive than astrophysical ones, it is always important to test alternative models of gravity at different scales.

The circular orbit approximation motivates future work in which noncircular orbits are considered from the beginning. In this context, it would be possible to study the loss of angular momentum and the effects of orbit circularization. This would be particularly interesting in quadratic gravity, where the presence of the Weyl-Weyl term generates the Ostrogradsky instability.

ACKNOWLEDGMENTS

L.G.M. is grateful to CNPq-Brazil (Grant No. 308380/2019-3) for partial financial support. M.F.S.A. acknowledges CNPq-Brazil for financial support. L.F.M.A.M.R. thanks CAPES-Brazil for financial support.

Appendix A: The gravitational energy-momentum tensor

In this Appendix, we calculate the gravitational energy-momentum tensor

$$t_{\mu\alpha} = -\frac{c^4}{8\pi G} \left[\langle G_{\mu\alpha}^{(2)} \rangle + \gamma \langle H_{\mu\alpha}^{(2)} \rangle - 2\alpha \langle I_{\mu\alpha}^{(2)} \rangle \right] \quad (\text{A1})$$

where $G_{\mu\alpha}^{(2)}$, $H_{\mu\alpha}^{(2)}$ and $I_{\mu\alpha}^{(2)}$ are given in Eqs. (50), (51), and (52), respectively.

The brackets $\langle \dots \rangle$ represent space-time averages of wave-like solutions obtained from Eqs. (14), (18), and (9). These averages are taken considering several periods of time and space in such a way that in these averages we can perform integrations by parts and neglect the surface terms [54]. Using this property, we will simplify $\langle H_{\mu\alpha}^{(2)} \rangle$ and $\langle I_{\mu\alpha}^{(2)} \rangle$. So, remembering that

$$\nabla_\mu \partial_\alpha R = \partial_\mu \partial_\alpha R - \Gamma^\rho_{\mu\alpha} \partial_\rho R,$$

we have for $\langle H_{\mu\alpha}^{(2)} \rangle$

$$\begin{aligned} \langle H_{\mu\alpha}^{(2)} \rangle &= \langle R^{(1)} R_{\mu\alpha}^{(1)} \rangle - \frac{1}{4} \eta_{\mu\alpha} \langle R^{(1)} R^{(1)} \rangle + \langle h_{\mu\alpha} \square R^{(1)} \rangle + \eta_{\mu\alpha} \langle [g^{\lambda\kappa} \nabla_\kappa \partial_\lambda]^{(1)} R^{(1)} \rangle + \langle \Gamma^{\rho(1)}_{\mu\alpha} \partial_\rho R^{(1)} \rangle \\ &= \langle R^{(1)} R_{\mu\alpha}^{(1)} \rangle - \frac{1}{4} \eta_{\mu\alpha} \langle R^{(1)} R^{(1)} \rangle + \langle h_{\mu\alpha} \square R^{(1)} \rangle - \eta_{\mu\alpha} \langle h^{\lambda\kappa} \partial_\kappa \partial_\lambda R^{(1)} \rangle - \eta_{\mu\alpha} \eta^{\lambda\kappa} \langle \Gamma^{\rho(1)}_{\kappa\lambda} \partial_\rho R^{(1)} \rangle \\ &\quad + \langle \Gamma^{\rho(1)}_{\mu\alpha} \partial_\rho R^{(1)} \rangle, \end{aligned}$$

where $\square = \partial^\sigma \partial_\sigma$. To obtain $\langle I_{\mu\alpha}^{(2)} \rangle$, we must develop the term

$$\begin{aligned} \langle (\nabla^\nu \nabla^\beta)^{(1)} C_{\mu\nu\alpha\beta}^{(1)} \rangle &= \langle (g^{\nu\kappa} \partial_\kappa \nabla^\beta)^{(1)} C_{\mu\nu\alpha\beta}^{(1)} \rangle - \langle (g^{\nu\kappa} \Gamma_{\kappa\mu}^\rho \nabla^\beta)^{(1)} C_{\rho\nu\alpha\beta}^{(1)} \rangle - \langle (g^{\nu\kappa} \Gamma_{\kappa\nu}^\rho \nabla^\beta)^{(1)} C_{\mu\rho\alpha\beta}^{(1)} \rangle \\ &\quad - \langle (g^{\nu\kappa} \Gamma_{\kappa\alpha}^\rho \nabla^\beta)^{(1)} C_{\mu\nu\rho\beta}^{(1)} \rangle \\ &= -\eta^{\beta\lambda} \langle h^{\nu\kappa} \partial_\kappa \partial_\lambda C_{\mu\nu\alpha\beta}^{(1)} \rangle - \eta^{\nu\kappa} \langle \Gamma_{\kappa\mu}^{\rho(1)} \partial^\beta C_{\rho\nu\alpha\beta}^{(1)} \rangle - \eta^{\nu\kappa} \langle \Gamma_{\kappa\nu}^{\rho(1)} \partial^\beta C_{\mu\rho\alpha\beta}^{(1)} \rangle \\ &\quad - \eta^{\nu\kappa} \langle \Gamma_{\kappa\alpha}^{\rho(1)} \partial^\beta C_{\mu\nu\rho\beta}^{(1)} \rangle. \end{aligned}$$

So, $I_{\mu\alpha}^{(2)}$ is written as

$$\begin{aligned} \langle I_{\mu\alpha}^{(2)} \rangle &= -\langle h^{\nu\kappa} \partial_\kappa \partial^\beta C_{\mu\nu\alpha\beta}^{(1)} \rangle - \eta^{\nu\kappa} \langle \Gamma_{\kappa\mu}^{\rho(1)} \partial^\beta C_{\rho\nu\alpha\beta}^{(1)} \rangle - \eta^{\nu\kappa} \langle \Gamma_{\kappa\nu}^{\rho(1)} \partial^\beta C_{\mu\rho\alpha\beta}^{(1)} \rangle - \eta^{\nu\kappa} \langle \Gamma_{\kappa\alpha}^{\rho(1)} \partial^\beta C_{\mu\nu\rho\beta}^{(1)} \rangle \\ &\quad + \frac{1}{2} \eta^{\nu\rho} \eta^{\beta\lambda} \langle R_{\rho\lambda}^{(1)} C_{\mu\nu\alpha\beta}^{(1)} \rangle. \end{aligned}$$

Therefore,

$$\langle G_{\mu\alpha}^{(2)} \rangle = \langle R_{\mu\alpha}^{(2)} \rangle - \frac{1}{2} \eta_{\mu\alpha} \langle R^{(2)} \rangle - \frac{1}{2} \langle h_{\mu\alpha} R^{(1)} \rangle, \quad (\text{A2})$$

$$\begin{aligned} \langle H_{\mu\alpha}^{(2)} \rangle &= \langle R^{(1)} R_{\mu\alpha}^{(1)} \rangle - \frac{1}{4} \eta_{\mu\alpha} \langle R^{(1)} R^{(1)} \rangle + \langle h_{\mu\alpha} \square R^{(1)} \rangle - \eta_{\mu\alpha} \langle h^{\lambda\kappa} \partial_\kappa \partial_\lambda R^{(1)} \rangle - \eta_{\mu\alpha} \eta^{\lambda\kappa} \langle \Gamma_{\kappa\lambda}^{\rho(1)} \partial_\rho R^{(1)} \rangle \\ &\quad + \langle \Gamma_{\mu\alpha}^{\rho(1)} \partial_\rho R^{(1)} \rangle, \end{aligned} \quad (\text{A3})$$

$$\begin{aligned} \langle I_{\mu\alpha}^{(2)} \rangle &= -\langle h^{\nu\kappa} \partial_\kappa \partial^\beta C_{\mu\nu\alpha\beta}^{(1)} \rangle - \eta^{\nu\kappa} \langle \Gamma_{\kappa\mu}^{\rho(1)} \partial^\beta C_{\rho\nu\alpha\beta}^{(1)} \rangle - \eta^{\nu\kappa} \langle \Gamma_{\kappa\nu}^{\rho(1)} \partial^\beta C_{\mu\rho\alpha\beta}^{(1)} \rangle - \eta^{\nu\kappa} \langle \Gamma_{\kappa\alpha}^{\rho(1)} \partial^\beta C_{\mu\nu\rho\beta}^{(1)} \rangle \\ &\quad + \frac{1}{2} \eta^{\nu\rho} \eta^{\beta\lambda} \langle R_{\rho\lambda}^{(1)} C_{\mu\nu\alpha\beta}^{(1)} \rangle. \end{aligned} \quad (\text{A4})$$

The next step is to calculate the various terms needed using decomposition (20). As $t_{\mu\nu}$ is calculated in vacuum, we can use the traceless-transverse gauge, and in this case, $\tilde{h} = \Psi = 0$ e $\square \tilde{h}_{\mu\alpha} = 0$. Then, the decomposed metric is rewritten as

$$\bar{h}_{\mu\alpha} = \tilde{h}_{\mu\alpha} + \Psi_{\mu\alpha} - \eta_{\mu\alpha} \Phi. \quad (\text{A5})$$

With these simplifications, the first-order quantities obtained in Sec. II simplify to

$$R^{(1)} \approx -3\square\Phi, \quad (\text{A6})$$

$$R_{\mu\alpha}^{(1)} \approx -\frac{1}{2} \square \Psi_{\mu\alpha} - \partial_\mu \partial_\alpha \Phi + \eta_{\mu\alpha} \square \Phi - \eta_{\mu\alpha} \frac{\Phi}{2\gamma}, \quad (\text{A7})$$

$$\begin{aligned} C_{\mu\nu\alpha\beta}^{(1)} &= \frac{1}{2} \left[\partial_\alpha \partial_\nu (\tilde{h}_{\mu\beta} + \Psi_{\mu\beta}) - \partial_\beta \partial_\nu (\tilde{h}_{\mu\alpha} + \Psi_{\mu\alpha}) + \partial_\beta \partial_\mu (\tilde{h}_{\nu\alpha} + \Psi_{\nu\alpha}) - \partial_\alpha \partial_\mu (\tilde{h}_{\nu\beta} + \Psi_{\nu\beta}) \right] \\ &\quad + \frac{1}{4} [\eta_{\mu\alpha} \square \Psi_{\nu\beta} - \eta_{\mu\beta} \square \Psi_{\nu\alpha} + \eta_{\nu\beta} \square \Psi_{\mu\alpha} - \eta_{\nu\alpha} \square \Psi_{\mu\beta}], \end{aligned} \quad (\text{A8})$$

$$\partial^\beta C_{\mu\nu\alpha\beta}^{(1)} = \frac{1}{4} [\partial_\mu \square \Psi_{\nu\alpha} - \partial_\nu \square \Psi_{\mu\alpha}], \quad (\text{A9})$$

and

$$\Gamma_{\kappa\mu}^{\rho(1)} = \frac{1}{2} \eta^{\rho\lambda} (\partial_\kappa h_{\lambda\mu} + \partial_\mu h_{\lambda\kappa} - \partial_\lambda h_{\kappa\mu}). \quad (\text{A10})$$

The term $\langle G_{\mu\alpha}^{(2)} \rangle$ is given by the Eq. (A2). The calculation of the terms $\langle R_{\mu\alpha}^{(2)} \rangle$ and $\langle R^{(2)} \rangle$ are extensive but straightforward and results in

$$\begin{aligned} \langle R_{\mu\alpha}^{(2)} \rangle &= -\frac{1}{4} \langle \partial_\mu \tilde{h}_{\nu\beta} \partial_\alpha \tilde{h}^{\nu\beta} \rangle - \frac{1}{4} \langle \partial_\mu \Psi_{\nu\beta} \partial_\alpha \Psi^{\nu\beta} \rangle + \frac{1}{2} \langle \partial_\alpha \Phi \partial_\mu \Phi \rangle - \frac{1}{2} \langle \partial_\mu \tilde{h}_{\nu\beta} \partial_\alpha \Psi^{\nu\beta} \rangle + \frac{1}{2} \langle \partial_\lambda \Psi_{\mu} \partial^\lambda \Psi_{\nu\alpha} \rangle \\ &\quad - \frac{1}{2} \eta_{\alpha\mu} \langle \partial^\lambda \Phi \partial_\lambda \Phi \rangle, \end{aligned} \quad (\text{A11})$$

and

$$\langle R^{(2)} \rangle = -\frac{9}{2} \langle \partial^\lambda \Phi \partial_\lambda \Phi \rangle - \frac{1}{4} \langle \partial_\lambda \Psi^{\nu\alpha} \partial^\lambda \Psi_{\nu\alpha} \rangle. \quad (\text{A12})$$

Substituting the results (A11), (A12), (A6), and (A5) in $\langle G_{\mu\alpha}^{(2)} \rangle$, we get

$$\begin{aligned} \langle G_{\mu\alpha}^{(2)} \rangle &= -\frac{1}{4} \langle \partial_\mu \tilde{h}_{\nu\beta} \partial_\alpha \tilde{h}^{\nu\beta} \rangle - \frac{1}{4} \langle \partial_\mu \Psi_{\nu\beta} \partial_\alpha \Psi^{\nu\beta} \rangle - \frac{1}{2} \langle \partial_\mu \tilde{h}_{\nu\beta} \partial_\alpha \Psi^{\nu\beta} \rangle + \frac{1}{2} \langle \partial_\alpha \Phi \partial_\mu \Phi \rangle \\ &\quad - \frac{1}{2} \langle \Psi^\nu{}_\mu \square \Psi_{\nu\alpha} \rangle - \frac{1}{4} \eta_{\mu\alpha} \langle \Phi \square \Phi \rangle - \frac{1}{8} \eta_{\mu\alpha} \langle \Psi^{\nu\beta} \square \Psi_{\nu\beta} \rangle + \frac{3}{2} \langle \Psi_{\mu\alpha} \square \Phi \rangle. \end{aligned} \quad (\text{A13})$$

The field equations (18) and (9) in vacuum can be written as

$$\square \Psi_{\mu\alpha} = \frac{1}{\alpha} \Psi_{\mu\alpha} \quad \text{and} \quad \square \Phi = \frac{1}{3\gamma} \Phi. \quad (\text{A14})$$

Substituting these equations into $\langle G_{\mu\alpha}^{(2)} \rangle$, we get

$$\begin{aligned} \langle G_{\mu\alpha}^{(2)} \rangle &= -\frac{1}{4} \langle \partial_\mu \tilde{h}_{\nu\beta} \partial_\alpha \tilde{h}^{\nu\beta} \rangle - \frac{1}{4} \langle \partial_\mu \Psi_{\nu\beta} \partial_\alpha \Psi^{\nu\beta} \rangle - \frac{1}{2} \langle \partial_\mu \tilde{h}_{\nu\beta} \partial_\alpha \Psi^{\nu\beta} \rangle + \frac{1}{2} \langle \partial_\alpha \Phi \partial_\mu \Phi \rangle \\ &\quad - \frac{1}{2\alpha} \langle \Psi^\nu{}_\mu \Psi_{\nu\alpha} \rangle - \frac{1}{12\gamma} \eta_{\mu\alpha} \langle \Phi^2 \rangle - \frac{1}{8\alpha} \eta_{\mu\alpha} \langle \Psi^{\nu\beta} \Psi_{\nu\beta} \rangle, \end{aligned} \quad (\text{A15})$$

where we use that $\langle \Psi_{\mu\alpha} \Phi \rangle = 0$. The relation $\langle \Psi_{\mu\alpha} \Phi \rangle = 0$ is derived from the vacuum field equations from the following construction:

$$\begin{aligned} \Phi \square \Psi_{\mu\alpha} &= \frac{1}{\alpha} \Phi \Psi_{\mu\alpha} \quad \text{and} \quad \Psi_{\mu\alpha} \square \Phi = \frac{1}{3\gamma} \Phi \Psi_{\mu\alpha} \Rightarrow \\ \langle \Phi \square \Psi_{\mu\alpha} - \Psi_{\mu\alpha} \square \Phi \rangle &= \left(\frac{1}{\alpha} - \frac{1}{3\gamma} \right) \langle \Phi \Psi_{\mu\alpha} \rangle \Rightarrow \\ \frac{1}{3\gamma\alpha} (3\gamma - \alpha) \langle \Phi \Psi_{\mu\alpha} \rangle &= 0. \end{aligned}$$

Thus, for $\alpha \neq 3\gamma$, we have $\langle \Phi \Psi_{\mu\alpha} \rangle = 0$. The quantity $\langle H_{\mu\alpha}^{(2)} \rangle$ is given by the Eq. (A3). Calculating each of the terms present in $\langle H_{\mu\alpha}^{(2)} \rangle$, we obtain

- First term:

$$\langle R^{(1)} R_{\mu\alpha}^{(1)} \rangle = \frac{3}{2} \langle \square \Phi \square \Psi_{\mu\alpha} \rangle + 3 \langle \square \Phi \partial_\mu \partial_\alpha \Phi \rangle - 3 \eta_{\mu\alpha} \langle (\square \Phi)^2 \rangle + \eta_{\mu\alpha} \frac{3}{2\gamma} \langle \Phi \square \Phi \rangle. \quad (\text{A16})$$

- Second term:

$$\langle R^{(1)} R^{(1)} \rangle = 9 \langle (\square \Phi)^2 \rangle. \quad (\text{A17})$$

- Third term:

$$\langle h_{\mu\alpha} \square R^{(1)} \rangle = -3 \langle \square \Psi_{\alpha\mu} \square \Phi \rangle - 3 \eta_{\alpha\mu} \langle (\square \Phi)^2 \rangle. \quad (\text{A18})$$

- Fourth term:

$$\langle h^{\lambda\kappa} \partial_\kappa \partial_\lambda R^{(1)} \rangle = -3 \langle (\square \Phi)^2 \rangle. \quad (\text{A19})$$

- Fifth term:

$$\eta^{\lambda\kappa} \langle \Gamma_{\kappa\lambda}^{\rho(1)} \partial_\rho R^{(1)} \rangle = -3 \langle (\square \Phi)^2 \rangle. \quad (\text{A20})$$

- Sixth term:

$$\left\langle \Gamma_{\mu\alpha}^{\rho(1)} \partial_\rho R^{(1)} \right\rangle = 3 \langle \partial_\mu \partial_\alpha \Phi \square \Phi \rangle - \frac{3}{2} \langle \square \Psi_{\alpha\mu} \square \Phi \rangle - \frac{3}{2} \eta_{\alpha\mu} \langle (\square \Phi)^2 \rangle. \quad (\text{A21})$$

Then we substitute these six results in the expression of $\langle H_{\mu\alpha}^{(2)} \rangle$ obtaining

$$\langle H_{\mu\alpha}^{(2)} \rangle = 6 \langle \square \Phi \partial_\mu \partial_\alpha \Phi \rangle - \frac{15}{4} \eta_{\mu\alpha} \langle (\square \Phi)^2 \rangle + \eta_{\mu\alpha} \frac{3}{2\gamma} \langle \Phi \square \Phi \rangle - 3 \langle \square \Psi_{\alpha\mu} \square \Phi \rangle. \quad (\text{A22})$$

Analogously to the case of $\langle G_{\mu\alpha}^{(2)} \rangle$, we can use the field equations (A14) and rewrite $\langle H_{\mu\alpha}^{(2)} \rangle$ as

$$\langle H_{\mu\alpha}^{(2)} \rangle = \frac{1}{\gamma} \left(\frac{1}{12\gamma} \eta_{\mu\alpha} \langle \Phi^2 \rangle - 2 \langle \partial_\mu \Phi \partial_\alpha \Phi \rangle \right), \quad (\text{A23})$$

where we use again that $\langle \Psi_{\alpha\mu} \Phi \rangle = 0$.

The quantity $\langle I_{\mu\alpha}^{(2)} \rangle$ is given by the Eq. (A4). Calculating each of the terms present in $\langle I_{\mu\alpha}^{(2)} \rangle$, we obtain:

- First term:

$$\langle h^{\nu\kappa} \partial_\kappa \partial^\beta C_{\mu\nu\alpha\beta}^{(1)} \rangle = -\frac{1}{4} \langle \square \Phi \square \Psi_{\mu\alpha} \rangle. \quad (\text{A24})$$

- Second term:

$$\eta^{\nu\kappa} \langle \Gamma_{\kappa\mu}^{\rho(1)} \partial^\beta C_{\rho\nu\alpha\beta}^{(1)} \rangle = \frac{1}{4} \langle \square \Psi^\lambda{}_\alpha \square \Psi_{\lambda\mu} \rangle + \frac{1}{4} \langle \square \Psi_{\mu\alpha} \square \Phi \rangle. \quad (\text{A25})$$

- Third term:

$$\eta^{\nu\kappa} \langle \Gamma_{\kappa\nu}^{\rho(1)} \partial^\beta C_{\mu\rho\alpha\beta}^{(1)} \rangle = -\frac{1}{4} \langle \square \Phi \square \Psi_{\mu\alpha} \rangle. \quad (\text{A26})$$

- Fourth term:

$$\eta^{\nu\kappa} \langle \Gamma_{\kappa\alpha}^{\rho(1)} \partial^\beta C_{\mu\nu\rho\beta}^{(1)} \rangle = \frac{1}{8} \left[\langle \square \Psi_{\lambda\alpha} \square \Psi_\mu{}^\lambda \rangle + \langle \square \Phi \square \Psi_{\mu\alpha} \rangle - \langle \partial_\mu \partial_\alpha \Psi_{\lambda\kappa} \square \Psi^{\kappa\lambda} \rangle \right]. \quad (\text{A27})$$

- Fifth term:

$$\frac{1}{2} \eta^{\nu\rho} \eta^{\beta\lambda} \langle R_{\rho\lambda}^{(2)} C_{\mu\nu\alpha\beta}^{(1)} \rangle = \frac{1}{8} \left(\langle \square \Psi_{\mu\beta} \square \Psi_\alpha{}^\beta \rangle + \langle \partial_\alpha \partial_\mu \Psi_{\nu\beta} \square \Psi^{\nu\beta} \rangle - \frac{1}{2} \eta_{\mu\alpha} \langle \square \Psi_{\nu\beta} \square \Psi^{\nu\beta} \rangle + \langle \square \Psi_{\mu\alpha} \square \Phi \rangle \right). \quad (\text{A28})$$

Substituting these five terms into $\langle I_{\mu\alpha}^{(2)} \rangle$, we get

$$\begin{aligned} \langle I_{\mu\alpha}^{(2)} \rangle &= \frac{1}{4} \langle \square \Phi \square \Psi_{\mu\alpha} \rangle - \frac{1}{4} \langle \square \Psi^\lambda{}_\alpha \square \Psi_{\lambda\mu} \rangle + \frac{1}{4} \langle \partial_\alpha \partial_\mu \Psi_{\nu\beta} \square \Psi^{\nu\beta} \rangle - \frac{1}{16} \eta_{\mu\alpha} \langle \square \Psi_{\nu\beta} \square \Psi^{\nu\beta} \rangle \\ &= -\frac{1}{4\alpha} \langle \partial_\mu \Psi_{\nu\beta} \partial_\alpha \Psi^{\nu\beta} \rangle - \frac{1}{4\alpha^2} \langle \Psi^\lambda{}_\alpha \Psi_{\lambda\mu} \rangle - \frac{1}{16\alpha^2} \eta_{\mu\alpha} \langle \Psi_{\nu\beta} \Psi^{\nu\beta} \rangle. \end{aligned} \quad (\text{A29})$$

Finally, to obtain the gravitational energy-momentum tensor $t_{\mu\alpha}$, we substitute Eqs. (A15), (A23) and (A29) in the expression (A1). Thus,

$$t_{\mu\alpha} = \frac{c^4}{8\pi G} \left[\frac{1}{4} \langle \partial_\mu \tilde{h}_{\nu\beta} \partial_\alpha \tilde{h}^{\nu\beta} \rangle - \frac{1}{4} \langle \partial_\mu \Psi_{\nu\beta} \partial_\alpha \Psi^{\nu\beta} \rangle + \frac{1}{2} \langle \partial_\mu \tilde{h}_{\nu\beta} \partial_\alpha \Psi^{\nu\beta} \rangle + \frac{3}{2} \langle \partial_\alpha \Phi \partial_\mu \Phi \rangle \right].$$

-
- [1] B.P. Abbott et al. Observation of gravitational waves from a binary black hole merger. *Phys. Rev. Lett.*, 116:061102, Feb 2016.
- [2] B.P. Abbott et al. GW170817: Observation of gravitational waves from a binary neutron star inspiral. *Phys. Rev. Lett.*, 119:161101, Oct 2017.
- [3] B.P. Abbott et al. Observation of gravitational waves from two neutron star–black hole coalescences. *The Astrophysical Journal Letters*, 915(1):L5, jun 2021.
- [4] Russell A Hulse and Joseph H Taylor. Discovery of a pulsar in a binary system. *The Astrophysical Journal*, 195:L51–L53, 1975.
- [5] Richard A. Isaacson. Gravitational radiation in the limit of high frequency. i. the linear approximation and geometrical optics. *Phys. Rev.*, 166:1263–1271, Feb 1968.
- [6] Richard A. Isaacson. Gravitational radiation in the limit of high frequency. ii. nonlinear terms and the effective stress tensor. *Phys. Rev.*, 166:1272–1280, Feb 1968.
- [7] Ryoyu Utiyama and Bryce S. DeWitt. Renormalization of a classical gravitational field interacting with quantized matter fields. *Journal of Mathematical Physics*, 3(4):608–618, 1962.
- [8] R P Woodard. How far are we from the quantum theory of gravity? *Reports on Progress in Physics*, 72(12):126002, nov 2009.
- [9] A.A. Starobinsky. A new type of isotropic cosmological models without singularity. *Physics Letters B*, 91(1):99–102, 1980.
- [10] Alan H. Guth. Inflationary universe: A possible solution to the horizon and flatness problems. *Phys. Rev. D*, 23:347–356, Jan 1981.
- [11] George Gamow. The evolutionary universe. *Scientific American*, 195(3):136–156, 1956.
- [12] Eleonora Di Valentino, Olga Mena, Supriya Pan, Luca Visinelli, Weiqiang Yang, Alessandro Melchiorri, David F Mota, Adam G Riess, and Joseph Silk. In the realm of the hubble tension—a review of solutions. *Classical and Quantum Gravity*, 38(15):153001, jul 2021.
- [13] Will Handley. Curvature tension: Evidence for a closed universe. *Phys. Rev. D*, 103:L041301, Feb 2021.
- [14] Eleonora Di Valentino, Alessandro Melchiorri, and Joseph Silk. Planck evidence for a closed universe and a possible crisis for cosmology. *Nature Astronomy*, 4(2):196–203, nov 2019.
- [15] Eleonora Di Valentino, Alessandro Melchiorri, and Olga Mena. Can interacting dark energy solve the H_0 tension? *Phys. Rev. D*, 96:043503, Aug 2017.
- [16] Sunny Vagnozzi. New physics in light of the H_0 tension: An alternative view. *Phys. Rev. D*, 102:023518, Jul 2020.
- [17] Eleonora Di Valentino, Alessandro Melchiorri, Olga Mena, and Sunny Vagnozzi. Nonminimal dark sector physics and cosmological tensions. *Phys. Rev. D*, 101:063502, Mar 2020.
- [18] Sunny Vagnozzi, Eleonora Di Valentino, Stefano Gariazzo, Alessandro Melchiorri, Olga Mena, and Joseph Silk. The galaxy power spectrum take on spatial curvature and cosmic concordance. *Physics of the Dark Universe*, 33:100851, sep 2021.
- [19] Sunny Vagnozzi, Abraham Loeb, and Michele Moresco. Eppur è piatto? the cosmic chronometers take on spatial curvature and cosmic concordance. *The Astrophysical Journal*, 908(1):84, feb 2021.
- [20] Thomas P. Sotiriou and Valerio Faraoni. $f(R)$ theories of gravity. *Rev. Mod. Phys.*, 82:451–497, Mar 2010.
- [21] Antonio De Felice and Shinji Tsujikawa. $f(R)$ theories. *Living Reviews in Relativity*, 13(1):3, jun 2010.
- [22] Shin’ichi Nojiri and Sergei D. Odintsov. Unified cosmic history in modified gravity: From theory to lorentz non-invariant models. *Physics Reports*, 505(2-4):59–144, aug 2011.
- [23] Salvatore Capozziello and Mariafelicia De Laurentis. Extended theories of gravity. *Physics Reports*, 509(4-5):167–321, dec 2011.
- [24] V. Ts. Gurovich and Alexei A. Starobinsky. Quantum Effects and Regular Cosmological Models. *Sov. Phys. JETP*, 50:844–852, 1979.
- [25] Aghanim et al. Planck 2018 results. *Astronomy & Astrophysics*, 641:A6, sep 2020.
- [26] Ted Jacobson and David Mattingly. Gravity with a dynamical preferred frame. *Phys. Rev. D*, 64:024028, Jun 2001.
- [27] Jacob D. Bekenstein. Relativistic gravitation theory for the modified newtonian dynamics paradigm. *Phys. Rev. D*, 70:083509, Oct 2004.
- [28] J W Moffat. Scalar–tensor–vector gravity theory. *Journal of Cosmology and Astroparticle Physics*, 2006(03):004–004, mar 2006.
- [29] R. R. Cuzinatto, C. A. M. de Melo, L. G. Medeiros, and P. J. Pompeia. Scalar-multi-tensorial equivalence for higher order $f(R, \nabla_\mu R, \nabla_{\mu_1} \nabla_{\mu_2} R, \dots, \nabla_{\mu_1} \dots \nabla_{\mu_n} R)$ theories of gravity. *Phys. Rev. D*, 93:124034, Jun 2016.
- [30] R. R. Cuzinatto, C. A. M. de Melo, L. G. Medeiros, and P. J. Pompeia. $f(R, \nabla_{\mu_1} R, \dots, \nabla_{\mu_1} \dots \nabla_{\mu_n} R)$ theories of gravity in einstein frame: A higher order modified starobinsky inflation model in the palatini approach. *Phys. Rev. D*, 99:084053, Apr 2019.
- [31] M Asorey, JL Lopez, and IL Shapiro. Some remarks on high derivative quantum gravity. *International Journal*

- of *Modern Physics A*, 12(32):5711–5734, 1997.
- [32] S. Nojiri, S.D. Odintsov, and V.K. Oikonomou. Modified gravity theories on a nutshell: Inflation, bounce and late-time evolution. *Physics Reports*, 692:1–104, 2017. Modified Gravity Theories on a Nutshell: Inflation, Bounce and Late-time Evolution.
 - [33] R.R. Cuzinatto, L.G. Medeiros, and P.J. Pompeia. Higher-order modified starobinsky inflation. *Journal of Cosmology and Astroparticle Physics*, 2019(02):055–055, feb 2019.
 - [34] G. Rodrigues-da Silva, J. Bezerra-Sobrinho, and L. G. Medeiros. Higher-order extension of starobinsky inflation: Initial conditions, slow-roll regime, and reheating phase. *Phys. Rev. D*, 105:063504, Mar 2022.
 - [35] J. Bezerra-Sobrinho and L. G. Medeiros. Modified starobinsky inflation by the $R \ln(\square) R$ term, 2022.
 - [36] Edgard C de Rey Neto, Odylio D Aguiar, and Jos C N de Araujo. A perturbative solution for gravitational waves in quadratic gravity. *Classical and Quantum Gravity*, 20(11):2025–2031, may 2003.
 - [37] Salvatore Capozziello and Francesco Bajardi. Gravitational waves in modified gravity. *International Journal of Modern Physics D*, 28(05):1942002, 2019.
 - [38] Tomohiro Inagaki and Masahiko Taniguchi. Gravitational waves in modified Gauss-Bonnet gravity. *International Journal of Modern Physics D*, 29(10):2050072, jul 2020.
 - [39] Louis Yang, Chung-Chi Lee, and Chao-Qiang Geng. Gravitational waves in viable $f(R)$ models. *Journal of Cosmology and Astroparticle Physics*, 2011(08):029–029, aug 2011.
 - [40] Patric Hölscher and Dominik J. Schwarz. Gravitational waves from inspiralling compact binaries in conformal gravity. *Physical Review D*, 99(8):084005, apr 2019.
 - [41] Chiara Caprini, Patric Hölscher, and Dominik J. Schwarz. Astrophysical gravitational waves in conformal gravity. *Physical Review D*, 98(8):084002, oct 2018.
 - [42] Joachim Näf and Philippe Jetzer. Gravitational radiation in quadratic $f(R)$ gravity. *Phys. Rev. D*, 84:024027, Jul 2011.
 - [43] S. Capozziello, M. De Laurentis, I. De Martino, M. Formisano, and S. D. Odintsov. Jeans analysis of self-gravitating systems in $f(R)$ gravity. *Phys. Rev. D*, 85:044022, Feb 2012.
 - [44] Salvatore Capozziello, Mariafelicia De Laurentis, and Valerio Faraoni. A bird’s eye view of $f(R)$ -gravity. *The Open Astronomy Journal*, 3(1):49–72, 2010.
 - [45] S. G. Vilhena, L. G. Medeiros, and R. R. Cuzinatto. Gravitational waves in higher-order R^2 gravity. *Phys. Rev. D*, 104:084061, Oct 2021.
 - [46] Yunho Kim, Archil Kobakhidze, and Zachary S. C. Picker. Probing quadratic gravity with binary inspirals, 2019.
 - [47] K. S. Stelle. Renormalization of higher-derivative quantum gravity. *Phys. Rev. D*, 16:953–969, Aug 1977.
 - [48] K. S. Stelle. Classical Gravity with Higher Derivatives. *Gen. Rel. Grav.*, 9:353–371, 1978.
 - [49] G. Rodrigues-da Silva and L. G. Medeiros. Second-order corrections to starobinsky inflation, 2022.
 - [50] P Teyssandier. Linearised $R + R^2$ gravity: a new gauge and new solutions. *Classical and Quantum Gravity*, 6(2):219–229, feb 1989.
 - [51] Pierre Teyssandier. New solutions in linearized $R + R^2$ gravity. *Astronomische Nachrichten*, 311(4):209–212, 1990.
 - [52] Patric Hölscher. Gravitational waves and degrees of freedom in higher derivative gravity. *Physical Review D*, 99(6):064039, mar 2019.
 - [53] Charalampos Bogdanos, Salvatore Capozziello, Mariafelicia De Laurentis, and Savvas Nesseris. Massive, massless and ghost modes of gravitational waves from higher-order gravity. *Astroparticle Physics*, 34(4):236–244, 2010.
 - [54] M. Maggiore. *Gravitational Waves: Volume 1: Theory and Experiments*. Gravitational Waves. OUP Oxford, 2008.
 - [55] Avijit Chowdhury, Semin Xavier, and S. Shankaranarayanan. Massive tensor modes carry more energy than scalar modes in quadratic gravity, 2022.
 - [56] H. Lü, A. Perkins, C. N. Pope, and K. S. Stelle. Spherically symmetric solutions in higher-derivative gravity. *Phys. Rev. D*, 92:124019, Dec 2015.
 - [57] H. Lü, A. Perkins, C. N. Pope, and K. S. Stelle. Black holes in higher derivative gravity. *Phys. Rev. Lett.*, 114:171601, Apr 2015.
 - [58] B.P. Abbott et al. Gw170104: Observation of a 50-solar-mass binary black hole coalescence at redshift 0.2. *Phys. Rev. Lett.*, 118:221101, Jun 2017.
 - [59] S. E. Woosley. Pulsational pair-instability supernovae. *The Astrophysical Journal*, 836(2):244, feb 2017.
 - [60] Maya Fishbach and Daniel E. Holz. Where are LIGO’s big black holes? *The Astrophysical Journal*, 851(2):L25, dec 2017.
 - [61] The LIGO Scientific Collaboration, The Virgo Collaboration, The KAGRA Collaboration, and R. et al. Abbott. The population of merging compact binaries inferred using gravitational waves through GWTC-3, 2021.
 - [62] José D. Edelstein, Rajes Ghosh, Alok Laddha, and Sudipta Sarkar. Causality constraints in quadratic gravity. *Journal of High Energy Physics*, 2021(9):150, sep 2021.
 - [63] Salvatore Capozziello and Christian Corda. Scalar gravitational waves from scalar-tensor gravity: production and response of interferometers. *International Journal of Modern Physics D*, 15(07):1119–1150, 2006.
 - [64] Christian Corda. Massive gravitational waves from the R^2 theory of gravity: Production and response of interferometers. *International Journal of Modern Physics A*, 23(10):1521–1535, apr 2008.
 - [65] Salvatore Capozziello, Christian Corda, and Maria Felicia De Laurentis. Massive gravitational waves from $f(R)$ theories of gravity: Potential detection with LISA. *Physics Letters B*, 669(5):255–259, nov 2008.
 - [66] Christopher P. L. Berry and Jonathan R. Gair. Linearized $f(R)$ gravity: Gravitational radiation and solar system tests. *Phys. Rev. D*, 83:104022, May 2011.
 - [67] D. J. Kapner, T. S. Cook, E. G. Adelberger, J. H. Gundlach, B. R. Heckel, C. D. Hoyle, and H. E. Swanson. Tests of the gravitational inverse-square law below the dark-energy length scale. *Phys. Rev. Lett.*, 98:021101, Jan 2007.